UNIVERSITY *of York*

This is a repository copy of *A limited role for unforced internal variability in 20th century warming.*.

White Rose Research Online URL for this paper:
https://eprints.whiterose.ac.uk/id/eprint/147408/

Version: Accepted Version

Article:

White Rose
university consortium
Universities of Leeds, Sheffield & York

eprints@whiterose.ac.uk
https://eprints.whiterose.ac.uk/

A limited role for unforced internal variability in 20th century warming.

Karsten Haustein[*] and Friederike E.L. Otto

Environmental Change Institute, University of Oxford, Oxford, United Kingdom

Victor Venema

Department of Meteorology, University of Bonn, Germany

Peter Jacobs

George Mason University, Department of Environmental Science and Policy, Fairfax, USA

Kevin Cowtan

Department of Chemistry, University of York, York, United Kingdom

Zeke Hausfather

Berkeley Earth, Berkeley, CA, USA; University of California Berkeley, Berkeley, CA, USA

Robert G. Way

Department of Geography and Planning, Queen's University, Kingston, ON, Canada

Bethan White

School of Earth and Atmosphere and Environment, Monash University, Melbourne, Australia

Aneesh Subramanian

Scripps Institution of Oceanography, San Diego, CA, USA

Andrew P. Schurer

School of Geosciences, University of Edinburgh, United Kingdom

[20] *Corresponding author address:* Karsten Haustein, Environmental Change Institute, University of

[21] Oxford, Oxford, United Kingdom

[22] E-mail: karsten.haustein@ouce.ox.ac.uk

ABSTRACT

The early 20th century warming (EW; 1910-1945) and the mid-20th century cooling (MC; 1950-1980) have been linked to both, internal variability of the climate system and changes in external radiative forcing. The degree to which either of the two factors contributed to EW and MC, or both, is still debated. Using a two-box impulse response model, we demonstrate that multidecadal ocean variability was unlikely to be the driver of observed changes in global mean surface temperature (GMST) after 1850 A.D. Instead, virtually all (97-98%) of the global low-frequency variability (> 30 years) can be explained by external forcing. We find similarly high percentages of explained variance for inter-hemispheric and land-ocean temperature evolution. Three key aspects are identified which underpin the conclusion of this new study: inhomogeneous anthropogenic aerosol forcing (AER), biases in the instrumental sea surface temperature (SST) datasets, and inadequate representation of the response to varying forcing factors. Once the spatially heterogeneous nature of AER is accounted for, the MC period is reconcilable with external drivers. SST biases and imprecise forcing responses explain the putative disagreement between models and observations during the EW period. As a consequence, Atlantic Multidecadal Variability (AMV) is found to be primarily controlled by external forcing too. Future attribution studies should account for these important factors when discriminating between externally-forced and internally-generated influences on climate. We argue that AMV must not be used as a regressor and suggest a revised AMV index instead (North Atlantic Variability Index; NAVI). Our associated best estimate for the transient climate response (TCR) is 1.57 K (± 0.70 at the 5-95% confidence level).

4

1. Introduction

The global temperature evolution over the instrumental period is conventionally attributed to the combination of external forcing and internal variability (Stott et al. 2000; Bindoff et al. 2013; Flato et al. 2013). Virtually all of the warming since 1950 is attributed to human influences (Stocker et al. 2013; Jones et al. 2013, 2016; Ribes et al. 2017). Yet due to the loosely constrained nature of magnitude and evolution of AER, there continues to be a fierce debate about the cause of multidecadal GMST fluctuations present in the instrumental record (Shiogama et al. 2006; Booth et al. 2012; Zhang et al. 2013; Thompson et al. 2015). Most prominently, the origin of the EW and MC periods, thought to be linked with North Atlantic (NA) ocean variability and commonly expressed in terms of AMV (Delworth and Mann 2000; Knight et al. 2005, 2006), is still hotly contested because of the difficulties to disentangle the contributions from internal and external drivers at different timescales (Brönnimann 2009; Mann et al. 2014; Zhang et al. 2016; Clement et al. 2016; Vecchi et al. 2017; Sutton et al. 2017; Hegerl et al. 2018).

Conventionally, the AMV has predominantly been attributed to internal ocean variability, which in turn has been linked to changes in the Atlantic Meridional Overturning Circulation (AMOC) as a deep ocean driving mechanism on multidecadal timescales (Zhang and Wang 2013; Yeager and Robson 2017). While stochastic atmospheric flux forcing is thought to influence SSTs on shorter timescales (Roberts et al. 2013; Duchez et al. 2016; Josey et al. 2019), associated with changes in the North Atlantic Oscillation (NAO) index (Hurrell and Deser 2009), the prevailing view regarding NA SST changes on longer timescales is that large internal variations are superimposed on the anthropogenic warming trend. However, in recent years, external forcing has been shown to contribute to multidecadal swings in the AMV region (Otterå et al. 2010; Murphy et al. 2017; Bellucci et al. 2017), suggesting a reduced role for internal ocean dynamics. Changes in

AER (Booth et al. 2012; Bellomo et al. 2018) as well as periods of strong volcanic activity (Iwi et al. 2012; Knudsen et al. 2014; Pausata et al. 2015; Swingedouw et al. 2017) have been linked to these changes. Also, it has been demonstrated that AMV-like SST pattern can be reproduced in slab-ocean experiments (Clement et al. 2015, 2016; Bellomo et al. 2018). Hence internally generated low-frequency GMST variations are increasingly thought to play only a smaller role, with Pacific ocean variability to be more recognised as a pacemaker for global temperature (Schurer et al. 2015; Dong and McPhaden 2017).

While there is no debate about the existence of aerosol-related dimming and brightening (Wild et al. 2007; Wild 2009) due to a huge array of supporting data from observations (Boers et al. 2017; Dumitrescu et al. 2017; Manara et al. 2017) and modelling (Shindell et al. 2013; Wilcox et al. 2013; Rotstayn et al. 2015; Dallafior et al. 2016; Chung and Soden 2017), its impact on the AMV is less certain. Many studies do not (Huss et al. 2010; Chylek et al. 2014) or insufficiently (Ting et al. 2009; Zhang et al. 2013) incorporate or acknowledge AER, which potentially leads to misattribution of cause (Zhang et al. 2016; O'Reilly et al. 2016) and effect (Chylek et al. 2009; Wyatt et al. 2012; Tung and Zhou 2013; Pasini et al. 2016; Levine et al. 2018). Arguments for the presence of an internally-generated AMV based on ostensible pseudo-oscillatory behaviour in instrumental, proxy, or model data are unconvincing (Singh et al. 2018), and it is noted that such behaviour can arise from statistical artefacts alone (Vincze and Jánosi 2011; Cane et al. 2017). Regression-based methods are thereby particularly susceptible to conflating internal variability with forced responses because of strong covariance between the predictors (Mann et al. 2014; Stolpe et al. 2017), yet studies that use the AMV as regressor or explanatory factor continue to be published despite the lack of an unequivocal physical underpinning (Lewis and Curry 2018; Rypdal 2018; Shen et al. 2018; Zhang et al. 2018; Folland et al. 2018).

6

We argue that any attribution exercise that does not sufficiently account for the spatio-temporal AER changes will invariably produce unreliable and erroneous results. Incorporating now better quantifiable biases in the instrumental SST record, we demonstrate that a carefully designed analysis (that avoids overfitting) yields a surprisingly high level of agreement between our model and observations without the need to infer additional unexplained internal variability. We endeavour to highlight the pitfalls associated with attributing and identify the shortcomings in representing the externally forced temperature responses.

Since attempts to estimate the magnitude of internal variability by means simple climate models are plagued from dissatisfying low correlations with observations (Aldrin et al. 2012; Skeie et al. 2014), here we use a refined two-box impulse response model framework which accounts for fast and slow responses to forcing perturbations in the climate system. To constrain the complexity of the model, we introduce a novel TCR adjustment factor for different forcing agents that is governed by robust physical factors. Apart from Northern Hemisphere (NHem) and GMST (Global), we also analyse Southern Hemisphere (SHem), land surface air temperature (Land) and SSTs (Ocean), expanding on previous GMST-only analyses (Mann et al. 2014; Dong and McPhaden 2017) to better understand the impact of radiative forcing changes on surface temperatures. We recommend all impulse response or energy balance model studies use land, ocean, and hemispheric temperature records with our dedicated set of model parameters as separate benchmark tests to robustly evaluate model performance.

2. Radiative forcing and observational data

We use the latest well-mixed greenhouse gas (WMGHG) radiative forcing (Etminan et al. 2016; Meinshausen et al. 2017) and the gridded aerosol community emission dataset (CEDS) (Hoesly et al. 2017), including sulphur dioxide (SO_2), ammonia (NH_3), black carbon (BC), and organic

carbon (OC). For solar forcing, we use sunspot numbers from the Greenwich Royal Observatory (Wilson and Hathaway 2006), scaled to solar forcing according to Dewitte and Nevens (2016). Stratospheric aerosol optical depth (AOD) data from explosive volcanic eruptions (Crowley et al. 2008; Crowley and Unterman 2013) are scaled to match NASA-GISS volcanic forcing data (Sato et al. 1993), and updated to include recent smaller eruptions (Vernier et al. 2011; Solomon et al. 2011; Arfeuille et al. 2014; Schmidt et al. 2018). Fig. 1a shows our revised forcing estimates.

The global direct radiative forcing for each aerosol component (SO_2, NH_3, BC, OC) is derived by scaling the current emissions to the AR5-forcing estimate for 2011 (Myhre et al. 2013; Stocker et al. 2013). Using BC emissions over North America, we account for enhanced Arctic warming during the first half of the 20th century (Johannessen et al. 2004; McConnell et al. 2007; Mc-Connell and Edwards 2008; Suo et al. 2013) (orange shading in Fig. 1b). The indirect forcing of -0.45W/m^2 is mostly a function of SO_2 (90%; 10% for OC). While considerable uncertainty regarding aerosol-cloud effects exist (Carslaw et al. 2013; Regayre et al. 2014; Nazarenko et al. 2017; Lohmann 2017), the best estimate for indirect AER in AR5 has not been fundamentally challenged since. Together with the direct effects, we obtain a total AER of $\sim$-0.55W/m^2 in accordance with AR5 (Fig. 1b), which is set to -0.75W/m^2 *pseudo-effective* global aerosol radiative forcing (ERF) in our response model framework (Fig. 1b, c). The total ERF estimate is guided by a recent review by Forest (2018), which is slightly lower than the best estimate for ERF of -0.9W/m^2 published in AR5. We note that other recent research has also suggested that AER ERF might be lower (Stevens 2015; Myhre et al. 2017), essentially reflecting arguments for stronger BC warming effects (Bond et al. 2013; Myhre and Samset 2015) and less cooling due to noticeable SO_2 reductions in China since 2006 (Smith et al. 2011; Klimont et al. 2013).

We use Berkeley Earth Land/Ocean (BE) (Rohde et al. 2012), HadCRUT4-Cowtan/Way (Cru4CW) (Cowtan and Way 2014; Cowtan et al. 2015), HadISST2 (Titchner and Rayner 2014;

8

Kennedy et al. 2017) and OSTIA (Donlon et al. 2012) as observational data. We note that there are indications that the land datasets may still underestimate warming in northern areas (Wang et al. 2017; Way et al. 2017). Since Cru4CW uses HadSST3 data (Kennedy et al. 2011) over oceans, we developed an additional composite product with Cru4CW over land and HadISST2 (1850-1985; preliminary release available only until 2010) and OSTIA data (1986-now; calibration period 1986-2005) over ocean to reflect the full range of available SST products (hereinafter referred to as HadOST). To obtain land and ocean proxies, ocean points that are covered with sea ice are treated as land points. The sea ice extent to generate the ice mask is taken from HadISST2 and OSTIA. The same mask is applied to Cru4CW and BE.

Due to continuous problems in currently available SST datasets, mainly manifest as warm bias as a result of changing SST sampling methods (from bucket to engine-room intake measurements) during World War II, associated with changing fleet composition (Karl et al. 2015; Hansen et al. 2016; Kent et al. 2017), Cowtan et al. (2017) have recently proposed a novel method to address the WWII bias using island and coastal weather stations only. Inspired by the idea, we replicate their analysis with a slightly simplified methodology. We use a mask where grid boxes over land (adjacent to ocean) and over ocean (along coastlines) are selected, including islands. The global average of all such subsampled ocean grid boxes establishes our new SST proxy. The two coastal time series are scaled to match the 1980-2016 global SST trend (see Cowtan et al. (2017) for details on the scaling method) as it is deemed the most reliable period in the marine instrumental record (Rahmstorf et al. 2017).

The results are shown in Fig. 1d for HadOST and BE and in Fig. 1e for ERSSTv4 and GHCNv3 as used in GISTEMP (Hansen et al. 2010). The scaling factors are provided in the figure legend. In both cases, the two coastal records (derived from HadISST2 and ERSSTv4) show excellent agreement during the calibration period. As expected, the land scaling factor is lower in agreement

9

with amplified warming trends over land. The land and ocean proxies agree after 1920 and show only minor deviations before 1920 (Fig. 1d). The HadOST proxies (land and ocean), suggest that HadISST2 is reliable with marginal biases between 1880-1940. We find much less agreement between GHCNv3 and ERSSTv4 before 1980. Our analysis further suggests that ERSSTv4 has a substantial cold bias between 1900-80 as well as a spurious warm bias during WWII (Fig. 1e). While by no means perfect, this straight-forward analysis is at least indicative that SSTs in general and ERSST in particular (versions 4 and 5 are almost identical throughout the period of coverage) are still impacted by substantial unresolved inhomogeneities. In our main analysis we discard GISTEMP and apply the following correction factors to HadOST, Cru4CW and BE during four of the WWII years (1942-45): NHem = -0.04°C, Global = -0.08°C, SHem = -0.12°C and Ocean = -0.18°C. The remaining years in the time series remain unchanged. We discuss the implications in section 4.

Finally, we use historical climate simulations from the Coupled Model Intercomparison Project (CMIP5) (Taylor et al. 2012) and an ensemble of the UK MetOffice HadCM3 model (Euro500) (Schurer et al. 2014) to estimate warming ratios and multidecadal internal variability.

3. Impulse response model and uncertainty

Following the method introduced in earlier work (Otto et al. 2015; Haustein et al. 2017), (vaguely similar to the analysis presented in Lean and Rind (2008) and Lean (2018)) we employ a two-box impulse response model framework that accounts for fast and slow temperature (T) changes in response to external forcing factors (*comp*: WMGHGs, anthropogenic aerosols (AER) and volcanic eruptions (VOL)). The fast component can be associated with the ocean mixed layer response whereas the slow component approximates the response of the deep ocean (Li and Jarvis 2009):

10

$$\frac{dT_j}{dt} = \frac{q_j \cdot F - T_j}{d_j}; T_{comp} = \sum_{j=1}^{2} T_j \tag{1}$$

$$
\begin{aligned}
TCR_{comp} \;=\; & F_{2xCO_2} \cdot \left(q_1 \cdot \left(1 - \frac{d_1}{70} \left(1 - e^{-\frac{70}{d_1}} \right) \right) \right. \\
& \left. + \; q_2 \cdot \left(1 - \frac{d_2}{70} \left(1 - e^{-\frac{70}{d_2}} \right) \right) \right)
\end{aligned}
\tag{2}
$$

$$ECS = F_{2xCO_2} \cdot (q_1 + q_2) \tag{3}$$

More details can be found in Millar et al. (2017). The forcing due to doubling of CO_2 (F_{2xCO_2}) is 3.71 W/m^2. The factor q_j (integrated contribution for response j) can be determined using Equation (2) and (3) with a defined set of values for TCR and ECS. Our chosen TCR range encompasses values from 1.1-2.1K, with an associated ECS range of 2.0-4.0K, in line with IPCC AR5 estimates (Stocker et al. 2013). As TCR/ECS-ratios derived from observational data are plagued by a variety of shortcomings (Armour 2017; Proistosescu and Huybers 2017; Marvel et al. 2018), we apply the CMIP5 mean of ∼0.53 as our central TCR/ECS-ratio estimate, supported, for example, by a reasonably good match of measured and simulated ocean heat uptake (Cheng et al. 2016). The associated adjustment factors for NHem, SHem, Land and Ocean as well as for AER and VOL forcing are introduced below.

The slow response time (d_2) is taken from Geoffroy et al. (2013a) (320 years), which included deep ocean feedbacks in contrast to accompanying work (Geoffroy et al. 2013b). Given that the fast response time (d_1) of 4 years suggested in the same study (Geoffroy et al. 2013a) relies on estimates from GCM simulations, we follow the approach presented in Rypdal (2012) and double d_1 to 8 years, which is in line with coefficients presented in Boucher and Reddy (2008) based on idealised simulations undertaken with the HadCM3 model. It is argued that observed

11

temperatures show a prolonged/delayed response due to mediating effects intrinsic to our climate system (Emile-Geay et al. 2008; Santer et al. 2014; McGregor et al. 2015) which may be less well represented in many GCMs (Le 2017). These estimates of d_1 and d_2 yield the highest correlation with observations.

As far as the response to AER is concerned, Shindell (2014) and Marvel et al. (2016) have highlighted the importance of different hemispheric treatment of the heterogeneous aerosol load. The conceptual idea is to have an enhanced TCR for AER due to its preponderance over land as a result of the skewed spatial distribution of aerosols. Differential heat capacities over land and ocean (and therefore implicitly the hemispheres) lead to considerably different response times over land and ocean, associated with inhomogeneous hemispheric warming rates that are mediated by cross-equatorial energy transports (Loeb et al. 2016; Stephens et al. 2016) for all forcing agents. Having said that, aerosols are transported over vast distances (Uno et al. 2009; Schulz et al. 2012), affecting oceans directly (due to albedo effect) and indirectly as well (due to cloud effects, particularly over formerly pristine areas), despite very low direct emissions over oceans mainly from ship exhaust (Kunkel et al. 2013; Shindell et al. 2013). Therefore, Ocean aerosol emissions are not a suitable proxy for the associated ocean temperature response. To remedy the problem, the inter-hemispheric exchange of aerosol-induced temperature responses has to be accounted for appropriately using coupling factors (introduced below).

The differential warming requires dedicated TCR calibration factors for the WMGHG, VOL and AER induced temperature responses. To obtain a plausible and robust set of such calibration factors, we use observed Transient Warming Ratios (TWR) between NHem and SHem as well as Land and Ocean. In Fig. 2, the temperature responses to total anthropogenic (a, b), WMGHG (c, d), AER (e, f) and VOL (g, h) are shown. Decadally averaged warming ratios are provided above

12

²²⁶ or under each graph. All data are low-pass filtered with an smoothing radius of 5 years. The TWR

²²⁷ is obtained during the 30 year period of strongest transient warming.

²²⁸ Given that TWRs for WMGHG, AER and VOL can only be inferred from GCMs, we apply a

²²⁹ scaling factor which represents the difference between observed and all-forcing TWRs. Assuming

²³⁰ that the observed TWR (red shaded area in Fig. 2a, b) is our target ratio, the responses in HadCM3

²³¹ are scaled accordingly. HadCM3 is used because it provides a small ensemble of simulations

²³² (mainly drawn from the Euro500 experiment) which is consistent across the experiments. The

²³³ TWR in the historical HadCM3 ensemble is 1.7, compared to 2.8 in HadOST (Fig. 2a). Hence a

²³⁴ scaling factor of ∼1.6 is applied to the TWR deduced from the WMGHG and AER ensemble of the

²³⁵ same model in order to correct for the underestimated TWR in the historical HadCM3 simulations.

²³⁶ The resulting inferred TWR (hereinafter referred to as TWRD; D = diagnosed), which is then used

²³⁷ in the response model, is provided in the boxes at the bottom of Fig. 2.

²³⁸ Since the bulk of the VOL response takes place on the fast timescale (1-10 years) and thus differ

²³⁹ from WMGHG related responses (Ding et al. 2014), we refrain from scaling and use the TWR

²⁴⁰ from HadCM3 directly (consistent with above-mentioned findings in Boucher and Reddy (2008)

²⁴¹ regarding HadCM3's fast response time). Note that the VOL responses in Fig. 2g, h are shown

²⁴² for the full 1500-1999 period in contrast to the shorter 1850-1999 (1850-2017) period for all other

²⁴³ scenarios.

²⁴⁴ In addition, since we do not know the resulting warming ratios in the response model a priori

²⁴⁵ when we impose the inferred TWRD, we compare them with the posteriori TWRs (hereinafter

²⁴⁶ referred to as TWRE; E = estimated) in order to validate our approach. We find that, for example,

²⁴⁷ the TWRD for WMGHGs (TCR of $2.65K$ over Land and $1.11K$ over Ocean) of ∼2.4 results in a

²⁴⁸ TWRE of ∼2.2 (see Fig. 2d). We therefore argue that our method is reasonably well constrained

²⁴⁹ to provide a robust answer.

13

All TCR calibration factors based on the deduced TWRDs (and shown at the bottom of Fig. 2) are summarised in the upper box in Fig. 3. We would like to point out that these calibration factors modulate the TCR/ECS ratio and are used for the full range of TCR and ECS values, respectively, not only the best estimate. The latter is provided at the top of Fig. 3 as well, together with the TCR for AER effective forcing which is ∼40% higher (best estimate = 2.2K) than that of WMGHGs (best estimate = 1.6K), consistent with findings in Rotstayn et al. (2015) and in pursuit to reflect the higher aerosols load over land.

To estimate the TCR calibration factor for AER, hemispheric and land-ocean coupling factors need to be determined. They reflect the above-mentioned fact that inter-hemispheric energy exchanges in response to the heterogeneous distribution of AER need to be balanced. Conveniently, the coupling factors are an emergent property and as such a function of the hemispheric area weighting factors, which are strictly interlinked and hence constrained as follows (example for WMGHGs):

$$
\begin{aligned}
T_{GHG}^{Global} &= 0.5 \cdot T_{GHG}^{NHem} + 0.5 \cdot T_{GHG}^{SHem} \\
&= 0.32 \cdot T_{GHG}^{Land} + 0.68 \cdot T_{GHG}^{Ocean}
\end{aligned}
\tag{4}
$$

Note that the Land fraction is marginally >30% because areas covered with sea ice are treated as land throughout the analysis. Apart from the area-weighted constraint, the coupling factors are also dependent on the emission ratio, i.e. the ratio between the hemispheric (and land/ocean) and the total global aerosol emission strength, which in turn determines the appropriate fractional contribution to match the inferred AER-TWRD (see Appendix A for more details). The resulting coupling factors are 3.9 (ratio of 1.47 and 0.38, which corresponds to 85% NHem and 15% SHem AER contribution for NHem AER and vice versa for SHem AER) and 2.1 (ratio of 1.46 and 0.7,

which corresponds to 70% Land and 30% Ocean AER contribution for Land AER and vice versa for Ocean AER). These factors are also provided in the bottom box of Fig. 3, together with all other parameters used in the response model. Global temperature trends for the 1978-2017 period in HadOST (a), CMIP5 (b) and HadCM3 (c) are also shown in Fig. 3. The spatial distribution of the trend highlights why observed and modelled TWR do not agree, which is primarily caused by delayed southern ocean warming (Armour et al. 2016), and partly by an accelerated Arctic amplification (Serreze and Barry 2011). Both physical processes are not satisfactorily reproduced in most GCMs.

Lastly, as apparent from the discrepancy between the AER factor provided at the bottom of Fig. 2 (3.5 and 2.4 for NHem/SHem and Land/Ocean, resp) and that shown in the top box of Fig. 3 (5.1 and 2.9 for NHem/SHem and Land/Ocean, resp), we increased the inferred AER-TWRD slightly. While the adjustment of the AER-TWRD does not change our conclusions (see Fig. S1 and S2 for the same result without AER-TWRD tuning), it does lead to better agreement between HadOST and the response model during the period of strongest AER cooling between 1960-80. Given that the HadCM3 AER ensemble is not a strict AER-only simulation rather then the difference between the *allforcing* and a non-aerosol ensemble of HadCM3, the results likely do not reflect the full extent of the aerosol-induced TWR. Therefore we think it is a defensible decision and well within the realm of the uncertainty of our AER-TWR estimate. The resulting AER timeseries is shown in Fig. 1c.

For the uncertainty analysis, response model, radiative forcing and internal variability uncertainty is considered. Apart from the TCR ($1.1...2.1K$) and ECS ($2.0...4.0K$) range, we also include a range of fast response times (3...13 years) in our response model uncertainty estimate. For the forcing, 200 total radiative forcing realisations are used (Forster et al. 2013) and converted into response model temperature equivalents to estimate the associated error range. The resulting σ

(32-68th percentiles) of the fractional uncertainties is shown in Fig. 4a (response model error in green and radiative forcing error in blue). If we assume that potential internally generated, low-frequency variability adds linearly to the externally forced response, we need an estimate of (modelled) unforced multidecadal variability. As introduced in Haustein et al. (2017), we use equidistant intervals of selected CMIP5 pre-industrial control simulations that do not drift (Knutson et al. 2013) and possess a similar range of unforced variability as our response model based estimate of the residual observational variability. In Fig. 4b, the low-pass filtered residuals for HadOST, Cru4CW and BE between 1850-2017 and low-pass filtered sample intervals of 168 years from selected CMIP5 models are shown together with their standard deviation (σ). The obtained 5-95th percentiles of their internal variability span $\pm 0.17^\circ$C ($\overline{\sigma}=0.1^\circ$C and $\overline{\sigma}^2=0.01^\circ$C^2) as shown in Fig. 4a in grey.

We note that there is additional parameter uncertainty, which is not fully included here as it is difficult to objectively constrain the upper and lower bounds of the respective parameters. In order to rectify this problem, in Fig. S3, we have plotted the response model results for a set of reasonable model parameters, including aerosol sensitivity, TWRs, coupling strength, TCR efficiency, varying SOL and VOL forcing, as well as high and low AER ERF (dashed line for -0.5 and -1.0 W/m^2). The resulting uncertainty is small compared to the total uncertainty, which is dominated by the forcing uncertainty. Hence we conclude that the our results are insensitive to the parameter choices, even if our observationally constrained estimates were biased.

4. Model performance and evolution

In Fig. 5, the response model results for Land (a; brown), NHem (b; red) and Global (c; green), Ocean (d; purple) and SHem (e; blue) are shown. The central *allforcing* temperature response estimate is shown as the bold line in the lower graph in each panel, while thin lines indicate slightly

16

higher/lower alternative TCR estimates as indicated at the right hand side ($1.2...2.0K$). The 5-95th percentiles and the inter-quantile (25-75th) uncertainties are added as shaded grey contours. The low-pass filtered (30 year smoothing radius) instrumental data from HadOST (dark green), Cru4CW (yellow) and BE (black) are shown for comparison, including the WWII correction introduced in section 2. Before filtering, the influence of ENSO (Deser et al. 2012) is removed from the observational timeseries in order to minimise short-term noise (Stuecker et al. 2015), following the multiple regression approach of Foster and Rahmstorf (2011).

Conversely, in the upper graphs in Fig. 5a - 5e we have added ENSO variability to the response model results by scaling the multivariate ENSO index (MEI) (Wolter and Timlin 1998) for each domain and applying the lag coefficient obtained from the multiple regression. Other than the WWII bias correction, the observational data in the upper graphs show the annual mean temperatures. On the top left in each panel, the explained variance (R^2) for non-ENSO corrected, model-adjusted (MEI), and observation-adjusted correlations between model and the observational datasets are shown. The correlations are based on the low-pass filtered timeseries (30 year smoothing radius). To avoid problems due to autocorrelation, the associated non-filtered R^2 between Global HadOST and model-adjusted (MEI) timeseries is 0.935 (not shown; 0.92 for Cru4CW and 0.912 for BE). We would like to highlight that our R^2 for HadOST exceeds the explained variance found in Rypdal (2018) and Folland et al. (2018), without the need to invoke any contribution of the contentious AMV.

We find excellent agreement between our response model and observations in all three timeseries. NHem and Land are well reproduced over the entire duration of the instrumental period, including the EW and the MC periods (Fig. 5a, 5b). SHem and Ocean are similarly well reproduced, with notable deviations before and after WWII when compared with Cru4CW or BE (Fig. 5d, 5e). Using HadOST, the SHem and Ocean model results can be almost entirely reconciled

17

with observations (Fig. 5d). HadOST and Ocean only start to diverge before 1900. But overall, the Global results (Fig. 5c) leave little room (of the order of $\sim 0.1^{\circ}$C) for unforced low-frequency temperature variations.

Before we investigate other notable excursions in light of the role of unforced Pacific and Atlantic ocean variability, in Fig. 6 the evolution of the response model for all five domains is shown. The top graph in each panel shows the response model result using WMGHG and aerosol forcing based on IPCC AR5 (Meinshausen et al. 2011), extrapolated to 2017, volcanic forcing from NASA-GISS (Sato et al. 1993) updated to 2017 and a fast response time of 4 years. As such, it corresponds to the results published in Haustein et al. (2017). The middle graph in each panel is using our slightly modified VOL and solar forcing and a fast response time of 8 years. All what is otherwise different compared to our final response model result as shown in the lower graph in each panel is AER. The results based on the new CEDS AER show significant improvements in each domain, resolving most of the discrepancies associated with the EW and MC period. As far as EW is concerned, the improved response model performance is partly linked with the SST bias correction during WWII which is only applied in the lower graph in Fig. 6. Accordingly, the warming spike particularly over Ocean (Fig. 6d) and SHem (Fig. 6e) disappears, leading to a visibly better agreement between model and observations.

With the current AER lowered by $>10\%$ (Fig. 1a), here we briefly explore the implications for TCR, including a cautionary remark regarding the lack of robustness when estimating ECS. In Fig. 5, the TCR range from 1.2-2.0K is indicated with our best estimate using a TCR of 1.6K (bold lines). Based on linear regression between HadOST and the Global response model result, our most precise TCR estimate is 1.57K with an associated inter-decile uncertainty range of 0.87-2.27K (10-90th percentiles). This is in good agreement with other recent work (Richardson et al. 2016), despite the lower AER estimate. While others have suggested that TCR might be

time-dependent (Gregory et al. 2015), our results do not provide evidence for a change over the instrumental period.

With the TCR/ECS-ratio held constant, ECS is tied to TCR by construction in our analysis (3.0*K* with an associated inter-decile uncertainty range of 1.7-4.3*K*). Nonetheless, it is instructive to investigate the impact of different ECS values upon the model results when the TCR/ECS ratio is permitted to vary. As shown in the lower graphs of Fig. 6 where we have added the response model result for the low-end (2.0*K*) and high-end (4.0*K*) ECS range, neither of the two estimates provides sufficient guidance as to which ECS value is more likely to be correct. The small range of possible outcomes severely hampers a robust ECS estimation. We therefore agree with others (Armour 2017; Proistosescu and Huybers 2017; Marvel et al. 2018) who found that ECS cannot reliably be inferred from historical observations alone, and recommend caution as ECS is easily conflated with the Effective Climate Sensitivity, the latter of which is likely to be lower (Knutti et al. 2017; Andrews and Webb 2018). Hence such attempts (Aldrin et al. 2012; Otto et al. 2013; Skeie et al. 2014; Lewis and Curry 2015; Mauritsen and Pincus 2017; Lewis and Curry 2018) should be viewed with extreme skepticism.

5. Role of unforced Pacific ocean variability

Returning to Fig. 5, here we assess a few noteworthy remaining excursions that are arguably related to unforced internal variability. To facilitate quantifying those excursions, in Fig. 7 the residuals between the HadOST and response model temperature timeseries are plotted for the five domains. In Fig. 7b, the low-pass filtered MEI evolution is provided (black line). Cru4CW and BE are shown in Fig. 7e for completeness.

We note that MEI shows signs of multidecadal variability, which is linked to the Pacific Decadal Variability (PDV) index (Newman et al. 2016; Henley 2017). Whether or not the unique behaviour

19

of the North Pacific variability (Williams et al. 2017; Kohyama and Hartmann 2017) and the associated observed strengthening of the Walker circulation (L'Heureux et al. 2013; McGregor et al. 2014; de Boisséson et al. 2014; Ma and Zhou 2016; Kajtar et al. 2017) are unforced or partly caused by changes in WMGHG (DiNezio et al. 2012; Xiang et al. 2014; Cai et al. 2015), AER (Dong et al. 2014; Takahashi and Watanabe 2016), or VOL (Emile-Geay et al. 2008; Le 2017) is a matter of intense debate and beyond the scope of this paper. However, the residuals as well as the explained variabilities provided in Fig. 5 suggest that low-frequency ENSO variability has little bearing on the outcome of our response model results. Merely the timing of the modern warming is slightly better aligned with observations when MEI rather than NINO3.4 (Trenberth 1997) is used (not shown), which is indicative of a minor role for additional decadal PDV impacts indeed.

Modelled Land (Fig. 7d) shows only a few peaks that are not explained by ENSO (e.g. 1884, 1913, 1939, 1949, 1980, 1991, 2010). Such excursions should be expected given the large standard deviation over land due to the stochastic nature of continental interannual variability (Mahlstein et al. 2012). There are a few years between 1950-60 which appear to be cooler than the response model suggests, but since no such deviation shows up over Ocean (see Fig. 7f), it might be related to European aerosol emissions (Persad and Caldeira 2018).

The positive residual after 2000 (also visible in the NHem residual in Fig. 7a) is perhaps more interesting as it relates to the infamously dubbed "hiatus" period in the wake of the strong El Niño in 1997/98. While primarily caused by a clustering of La Niña events around 2010 (Kosaka and Xie 2013; England et al. 2014; Schurer et al. 2015; Dong and McPhaden 2017), upon closer inspection another feature stands out. There has been a succession of anomalously cold years between 2010-2013, which is exclusively linked with boreal winter. More precise, this period is linked with extremely cold Eurasian winters (Cohen et al. 2012) which may or may not have been assisted by forced atmospheric circulation changes in response to declining sea ice (Tang

et al. 2013; Cohen et al. 2014; Overland 2016; Francis 2017; Hay et al. 2018). But other than that, SHem (Fig. 7c) and Ocean (Fig. 7f) residuals are inconspicuously smooth and only diverge before 1900 as outlined above already. Overall, our results support previous work that has shown that using updated external radiative forcing (Huber and Knutti 2014; Schmidt et al. 2014) and accounting for ENSO-related variability explains the so-called "hiatus". We refer to Medhaug et al. (2017) for a comprehensive review of the unprecedented flurry of publications on the subject. That said, despite being less sensitive to small changes near the endpoints compared to higher degree polynomial fits, we caution that the lowess smoother is still susceptible to overestimating trend changes at the beginning and end of the time series.

With explained variabilities ∼98% for HadOST for the Land (Fig. 5a), NHem (Fig. 5b) and Global (Fig. 5c) response model results, we conclude that almost all low-frequency variability is explained by external forcing factors independent of ENSO. The Ocean (Fig. 5d) and SHem (Fig. 5e) results reveal similar explanatory skill with explained variabilities between 93-95%. Interestingly, BE shows lower correlation factors than Cru4CW over Ocean (even more so over SHem), despite their common use of HadSST3. Thus, differences in data processing alone can explain much of the discrepancies. The fact that HadOST not only fares considerably better in terms of correlation, but also performs best regarding the coastal proxy analysis (Fig. 1d), justifies its inclusion in our analysis. However, more work needs to be done to reconcile the differences between the available SST products and to reduce associated biases (Davis et al. 2019). In Appendix B, we briefly analyse the spatio-temporal characteristics of those products with regard to decadal means.

6. Role of unforced Atlantic ocean variability

While the accurate reproduction of the EW and MC period in our response model framework does not require multidecadal temperature variability to attribute to the ostensible AMV, we do not dispute the existence of internal variability associated with AMOC variations. Therefore here we aim at quantifying the AMOC's role in setting NHem temperatures and its relation to the AMV. In order to facilitate the assessment, we would like to propose a more adequate, straight-forward and intuitive definition of the AMV index itself. Rather than using the standard definition (Delworth and Mann 2000) or an improved definition thereof (van Oldenborgh et al. 2009), we define the AMV as average SST at 25-60°N and 7-75°W (red box in Fig. 8d) minus NHem temperature. The resulting revised timeseries is shown in Fig. 7a (bold black line).

The revised AMV index (which we more appropriately propose to be named *North Atlantic Variability Index* or NAVI) is essentially reflecting and reliably mirroring the long-term AMOC decline in response to anthropogenic warming. The unprecedented dip aound 2015 is associated with the continued advection of very cold air of Arctic origin over the Canadian archipelago region during the winters of 2014/15 and 2015/16. Atmospheric forcing has been recognised to drive short-term AMOC variability (Roberts et al. 2013; Duchez et al. 2016) as opposed to gradual changes in sea ice cover (Sévellec et al. 2017), temperature, salinity and pressure gradients that eventually cause the slower long-term AMOC changes that are indeed already detectable Rahmstorf et al. (2015) and concomitant with the well-known Atlantic Warming Hole (AWH) (Menary and Wood 2018). Arguably, asymmetric land-ocean warming is a more mundane explanation for the colder NA region relative to NHem, as it is physically consistent with a transient warming scenario, but the slow pace of the NAVI decline suggests a contributing role for AMOC.

In order to qualitatively explore the role of longer-term effects associated with low-frequency modes of variability, we have conducted a simple correlation analysis. In Fig. 8, we have plotted the spatial map of correlation coefficients between Global and NHem timeseries obtained from the response model versus global observations (HadOST). The correlation between the older, slightly more advanced AMV index (van Oldenborgh et al. 2009) and HadOST is provided as well (Fig. 8d, g, k). We notice that the AWH in the subpolar NA region appears uncorrelated with the forcing timeseries (Fig. 8a, b, e), regardless whether we use the Global or NHem timeseries. Another noteworthy feature is the accompanying anti-correlation between the AMV index and most world regions.

Since we are not aware of a robust mechanism that would cause multidecadal AWH variability as opposed to a steady decline, in the following we test three potential reasons for why the AWH region may or may not follow externally forced changes: (1) A long-term warming trend difference, (2) a different spectrum of high-frequency SST variability, or (3) true internal low-frequency variability. To investigate whether (3) is a viable explanation, we applied running means from 5-20 years (Fig. 8e, h, m; middle panel), we linearly detrended model and observations (Fig. 8c), or we did both (Fig. 8f, j, n; rhs panel).

What we find is that the AWH is robust against temporal averaging as far as non-detrended data are concerned. In contrast, if detrended data are used, the temporal averaging aligns the NAVI/AWH region with the NHem forcing response in terms of correlation, maintaining its (forced) multidecadal low-frequency variability. In fact, detrending alone considerably reduces the unique behaviour of the AWH region already (Fig. 8c). What we infer from this is that the secular warming trend (1) is responsible for the specific characteristic of the AMV region. The root cause of this cooling trend is well known and one of the key features in GCM projections (Rahmstorf et al. 2015; Menary and Wood 2018). The high-frequency variability over the wider

23

NA region is higher than on global average, but comparable in magnitude to the western North Pacific (equally high supply of baroclinicity) or Eurasia (Fig. 8b).

After a decade, not much multi-annual stochastic variability is left (Fig. 8e). Together with the Indian ocean, the wider NA region shows high correlations with the NHem model after trend removal in both (Fig. 8f), suggesting substantial dependencies on externally forced low-frequency variability. It is a different story over land (and much of the Pacific), where the signal-to-noise ratio is lower on decadal scales due to limited radiative constraints on winter temperatures (Cohen et al. 2012; Knutson et al. 2013; Deser et al. 2017). The positive correlation between the 20 year low-pass filtered, detrended AMV and the Arctic (Fig. 8k) is physically very plausible as amplified Arctic warming relies on heat transport via the NA region, governed by the NAO index and the associated strength of the AMOC. However, it is the forced long-term warming trend that is the driver as evident from Figs. 8m and 8n.

Since no noticeable low-frequency signal can be detected over the key AWH region (Fig. 8n), we conclude that it is unlikely that internal variability on timescales > 5 years plays an important role in the North Atlantic. There is room for 1-5 year unforced feedbacks, but apart from the cooling due to the long-term decline in AMOC strength (Fig. 8m), high- and low-frequency AMV pattern appear to be externally forced according to our response model results. This is in line with an empirical model study that uses multiple regression to attribute forcing contributions globally (Suckling et al. 2017), and also supported by other studies that show that subpolar NA variability is largely driven by AMOC changes, with little evidence for a strong AMV-AMOC link (Marini and Frankignoul 2014; Frankignoul et al. 2017).

In conclusion, combined with the recent downward trend in the new NAVI index, our analysis strongly suggests that the impact of internally generated NA ocean dynamics on Global, NHem and Land temperatures is rather limited. Remaining AMOC related to low-frequency variability

24

(Zhang 2017) may have regional implications, but a strong influence beyond that is unlikely. The results are supported by another simple exercise in which NA SSTs are weighted by the surface area of the AMV/NAVI region, divided by the NHem surface area. This way, the fractional fingerprint of the AMV on NHem temperatures can be inferred. The peak contribution would be $<0.03^{\circ}$C, assuming all NA SST variability is of internal origin, which we have shown not to be a very plausible conjecture. Helped by a more advanced (yet still debatable) regression analysis, we note that Folland et al. (2018) also found almost no AMV contribution to global temperature.

7. Conclusions

With explained variabilities of observed global temperatures of up to 98% (30 year smooth) or $\sim$93% (with ENSO variability), respectively, our impulse response model performs exceptionally well. We are able to match the historical temperature evolution since at least 1850 in general, and succeed in reproducing both the EW and the MC period with high precision in particular, without the need to invoke unexplained internal multidecadal temperature variability as an additional driver.

Three key aspects are crucial for an appropriate attribution of the temperature response to external radiative forcing perturbations. (1) Careful treatment of the spatially heterogeneous AER forcing as its temporal evolution has major repercussions for both the EW and the MC period. (2) Removal of the WWII warm bias in the current generation of SST datasets as there is now solid evidence that 1942-1945 period is biased warm to differing degrees, causing a spurious warming trend at the end of the EW period. (3) Calibration of the fast response time in order to account for the mediating effects of ENSO as far as the response to volcanic eruptions is concerned.

While others (Mann et al. 2014; Folland et al. 2018) have found similarly good agreement as far as the GMST evolution is concerned, our analysis demonstrates that it is possible to reproduce

25

the temperature evolution separately for NHem, SHem, Land and Ocean with equal precision. We achieve this by introducing a set of suitable TCR calibration factors that are informed by observed (HadOST) and modelled (HadCM3) TWRs and traceable throughout the analysis. Apart from minor fine-tuning related to the deduced TWR for AER, every response model parameter used in our study is backed up by independent analysis and/or based on well-established research. The use of updated aerosol emission and volcanic forcing data as well the application of a longer fast response time (complemented by a hemispherically more uniform fast VOL response) are otherwise the only changes that we made compared to previous iterations within the response model framework. Owing to the introduced analytical constraints, which are designed to avoid model tuning, our results warrant robustness against overfitting.

With the introduction of HadOST, which includes a coastal temperature analysis inspired by Cowtan et al. (2017) that appears least biased with regard to the incorporated HadISST2 and OS-TIA SSTs, we add another option to the existing batch of GMST datasets. We recommend to use it more widely as it resolves some of the discrepancies present in HadSST3 before 1940. Despite a smaller warm bias during WWII in HadISST2 compared to HadSST3, we still have to impose a correction factor (-0.08°C for GMST) to reconcile it with the coastal hybrid temperature time-series. As a result, almost all of the EW warming could ultimately explained by external forcing changes, which - if confirmed by future research - may call the current partition of attributable EW causes, as recently reviewed in Hegerl et al. (2018), in considerable doubt.

In our assessment of potential contributions from Atlantic and Pacific multidecadal variability, we demonstrate that with the exception of prolonged periods of El Niño or La Niña preponderance, there is little room for internal unforced ocean variability beyond subdecadal timescales, which is particularly true for the NA region. This finding is buttressed by our demonstration that despite high co-variability, cause (VOL and AER) and effect (AMV) are clearly distinguishable. That

26

does not mean AMV cannot have internal mechanisms (Zhang 2017), rather only that the signal cannot be detected in Global or NHem (nor is necessary to explain their temporal evolution). Hence the traditional AMV index must not be used as predictor or explanatory variable, as it may lead to demonstrably incorrect or flawed attribution results (Hetzinger et al. 2008; Chylek et al. 2009; Huss et al. 2010; Wyatt et al. 2012; Tung and Zhou 2013; Chylek et al. 2014; Pasini et al. 2016; Hodgkins and Wilson 2017; Yan et al. 2017; Shen et al. 2018; Zhang et al. 2018). We suggest a revised AMV index formulation (NAVI) which avoids such pitfalls as it better mirrors the long-term AMOC decline as suggested, for example, in (Rahmstorf et al. 2015).

On that note, we also caution against confusing atmospherically driven short-term variability (noise) with changes due to anthropogenic or natural external forcing factors (signal). As demonstrated in the supplementary analysis, anomalous atmospheric NHem winter circulation features explain most of the short-term AMOC variability, acting as the control knob on multi-monthly timescales. Longer timescales are conceivable: (1) Via changing wind stress related to anomalous NAO phasing, which in turn affects the subpolar horizontal gyre circulation (Piecuch et al. 2017). (2) Via atmospheric teleconnections associated with ENSO such as the PNA-NAO relationship (Pinto et al. 2011), which in turn links to the emerging paradigm of the Pacific basin as pacemaker for global temperature (Guan and Nigam 2009; Kosaka and Xie 2013; England et al. 2014; Schurer et al. 2015; Dong and McPhaden 2017; Frankignoul et al. 2017). (3) Via *ocean memory* effects, which may favour the reoccurrence of certain large-scale weather patterns in the Euro-Atlantic region during successive boreal winter seasons via air-sea coupling (Scaife et al. 2014). But generally, progress in understanding Atlantic decadal climate variability has been slow (Yeager and Robson 2017). Taken together, our analysis underscores that despite the complexities of the climate system, changes to the mean state are dominated by radiative forcings on longer timescales and ENSO-related variability on shorter timescales.

27

By virtue of these findings, we are confident that our associated best TCR estimate of 1.57 (± 0.70) K is robust, despite a substantial error range due to the large forcing uncertainty. We strongly advise against the use of ECS estimates based on the instrumental record alone without considering further evidence (from paleo-archives or GCMs), as they cannot be reliably constrained with data of such a short time interval.

In a future analysis, we aim to quantify another important response model feature which also contributes to an improved representation of the EW period. In a nutshell, it can be demonstrated that failure to initialise the response model (or GCMs for that matter) before a series of strong volcanic eruptions will very likely bias the beginning of the simulated EW period warm, leading to an artificially low warming trend in models.

APPENDIX A

Calculation of coupling factors

As outlined in Section 3, inter-hemispheric energy exchanges in response to the heterogeneous distribution of AER need to be balanced by virtue of so-called coupling factors. As shown in Fig. 3, for AER there is a notable discrepancy between the TCR scaling factors (2.5/1.9 for NHem/SHem and 2.7/1.95 for Land/Ocean) and the diagnosed AER-TWR (5.1 for NHem/SHem and 2.9 for Land/Ocean). A discrepancy that does not appear for WMGHG and VOL (for instance: TWRD$_{WMGHG}$ = 2.23/0.97 = 2.3). This is where the coupling factor comes into play. Since the TCR scaling only works under the assumption that the NHem aerosol response is governed by NHem aerosol emissions (and vice versa for SHem; same problem for Land and Ocean), we have to find a way to accommodate the additional temperature response from SHem emissions in case of the NHem response.

We have applied two-stage methodology: (1) We derive the emission ratio, i.e. the ratio between the hemispheric (and land/ocean) and the total global aerosol emission strength. It is a function of the fractional contribution of each hemisphere (or land/ocean) and could vary between 95% to 5%, up until 50% to 50%. (2) We determine the optimal fractional contribution or coupling strength. For this to work, we balance the ratio of the TCR scaling factors (e.g. 2.5 for NHem and 1.9 for SHem) and the TWRD (e.g. 5.1 for NHem/SHem). Since the effective forcing of the SHem emissions will be lower (due to the lower TCR scaling factor), a secondary scaling factor has to be applied to NHem and SHem emission strength. This factor is only be equal for one particular set of coupling strengths. For NHem/SHem, the fractional contributions are 85% and 15%, associated with a NHem emission ratio (fractional NHem emission divided by Global emissions) of 1.58 and a SHem emission ratio (fractional SHem emission divided by Global emissions) of 0.42. The

29

additional secondary scaling factor is 0.93. Hence the NHem/SHem emission ratio is reduced to 1.47 and 0.38. Their ratio defines the coupling factor, which is 3.9 accordingly (=1.47/0.38).

Applying the same method for Land/Ocean, the fractional contributions are 70% and 30%, associated with a Land emission ratio (fractional Land emission divided by Global emissions) of 1.35 and an Ocean emission ratio (fractional Ocean emission divided by Global emissions) of 0.65. The secondary scaling factor is 1.08, which is explained by the fact that the Ocean sensitivity is lower, but instead covers a much larger area fraction compared to Land (area fractions are equal in case of NHem/SHem). Hence the Land/Ocean emission is increased to 1.46 and 0.70. The associated ratio to determine the coupling factor is 2.1 (see lower box in Fig. 3 and fine-print below it).

APPENDIX B

Decadal temperature evolution

As highlighted in the main text, SST observations are still afflicted with considerable uncertainties. Having investigated time series of field means, here we provide the spatiotemporal context and discuss potential causes for some of the discrepancies noted above. In Fig. B1, the GMST dataset used in this study are plotted as decadal average from 1850-1859 to 2010-1817 (BE, Cru4CW, HadOST), accompanied by GISTEMP during 1880-1889 to 2010-2017. In addition, the 20th Century reanalysis (20C Rean) (Hirahara et al. 2014), the ensemble mean of a subset of CMIP5 simulations are plotted, together with NorESM1-M (Bentsen et al. 2013) which is found to represent the temperature evolution since 1850 very well compared to observations. We also added the recently proposed Hybrid SSTs (Cowtan et al. 2017). The decade 1940-1949 is highlighted by the red box. Note that HadOST and Cru4CW use the same infilled HadCRUT4 (Morice et al. 2012) data over land. We also note that both, Cru4CW and BE have shown to carry a small

negative trend bias in recent years (Hausfather et al. 2017). If that is not enough, it has also been suggested that the Arctic region might still be biased cold (Wang et al. 2017; Way et al. 2017).

As noted above, the 1880-1935 period is too cold in HadSST3 (Cru4CW) compared to HadISST2 (HadOST), most pronounced during 1890-1920. Looking at those three decades, at least the first two show a noteworthy feature near Cape Cauldron off the southern tip of South Africa, presumably associated with the Agulhas and Brazil currents. The otherwise distinct cold SST anomalies in the turbulent exit region where the Agulhas current leaks into the South Atlantic ocean (compare HadOST) turns into a vast area of cold SST anomalies that essentially covers most of the South Atlantic. Given the poor observational coverage and the intrinsic shortcomings of any infilling technique (Kriging in case of Cru4CW), it is likely that the cold South Atlantic SST anomalies in Cru4CW, BE and GISTEMP are exaggerated to varying degrees.

Since the only bias in HadOST with regard to our response model results was found during the 1850-1879 period, mainly caused by warmer NH SST conditions, it is interesting to ask whether the warm SST anomaly in the North Pacific in HadOST is real given it does not show up in other observational datasets. While such a pattern is consistent with a prolonged PDV negative phase, the amplitude of the anomaly appears very strong, especially during the 1860s. The pattern re-occurs during the 1950-80 period, but background SSTs are less cold than during the 1850-79 period. This is arguably a feature which deserves to be investigated in more detail, particularly in light of recent work by Huang et al. (2018).

Regarding the WWII period, even though we have plotted decadal averages, what stands out is the sudden warming of all ocean basins in ERSST during the 1940s (and to a much lesser extent HadSST3 and HadOST). As evident from Fig. 5a, Land did not notably warm during the same period, which strongly suggests an artifactual feature, related to biases due to the previously explained change in fleet composition during WWII. The final feature we would like to mention

31

concerns the cold bias during 1950-80 in ERSST. While the general NHem ocean cooling due to increased anthropogenic SO_2 emissions is visible in all observations (and CMIP5 simulations, irrespective of some temporal misalignments), ERSST seems to exaggerate the cooling slightly given that the spatial pattern of the SST anomalies are indistinguishable from other datasets. We speculate that this might be a general theme in ERSST given that it draws heavily from maritime nighttime measurements in contrast to other products. We note that ERSSTv5 (Huang et al. 2017) has not changed notably compared to ERSSTv4.

As we cannot provide robust conclusions with regard to causes for the mismatch between different observational dataset at this point, we would like to close by encouraging the research community to address the oftentimes under-appreciated problems in more depth. Insights from energy balance models such as presented in this study can guide such efforts. With clever new strategies to combine the various information available, we are confident that the remaining gaps in our understanding will be eliminated and instrumental data brought into better agreement.

References

Aldrin, M., M. Holden, P. Guttorp, R. Skeie, G. Myhre, and T. Berntsen, 2012: Bayesian estimation of climate sensitivity based on a simple climate model fitted to observations of hemispheric temperatures and global ocean heat content. *Environmetrics*, **23 (3)**, 253–271.

Andrews, T., and M. Webb, 2018: The Dependence of Global Cloud and Lapse Rate Feedbacks on the Spatial Structure of Tropical Pacific Warming. *Journal of Climate*, **31**, 641–654.

Arfeuille, F., D. Weisenstein, H. Mack, E. Rozanov, T. Peter, and S. Brönnimann, 2014: Volcanic forcing for climate modeling: a new microphysics-based data set covering years 1600–present. *Climate of the Past*, **10**, 359–375, doi:10.5194/cp-10-359-2014.

Armour, K., 2017: Energy budget constraints on climate sensitivity in light of inconstant climate feedbacks. *Nature Climate Change*, **7**, 331–335.

Armour, K., J. Marshall, J. Scott, A. Donohoe, and E. Newsom, 2016: Southern Ocean warming delayed by circumpolar upwelling and equatorward transport. *Nature Geoscience*, **9**, 549–554.

Bellomo, K., L. Murphy, M. Cane, A. Clement, and L. Polvani, 2018: Historical forcings as main drivers of the Atlantic multidecadal variability in the CESM large ensemble. *Climate Dynamics*, **50 (9-10)**, 3687–3698.

Bellucci, A., A. Mariotti, and S. Gualdi, 2017: The role of forcings in the 20th century North Atlantic multi-decadal variability: the 1940-1975 North Atlantic cooling case study. *Journal of Climate*.

Bentsen, M., and Coauthors, 2013: The Norwegian Earth System Model, NorESM1-M - Part 1: Description and basic evaluation of the physical climate. *Geoscientific Model Development*, **6**, 687–720.

Bindoff, N. L., and Coauthors, 2013: *Detection and Attribution of Climate Change: from Global to Regional. In: Climate Change 2013: The Physical Science Basis. Contribution of Working Group I to the Fifth Assessment Report of the Intergovernmental Panel on Climate Change.* Cambridge University Press, Cambridge, United Kingdom and New York, NY, USA.

Boers, R., T. Brandsma, and A. Pier Siebesma, 2017: Impact of aerosols and clouds on decadal trends in all-sky solar radiation over the Netherlands (1966-2015). *Atmospheric Chemistry and Physics*, **17**, 8081–8100.

Bond, T., and Coauthors, 2013: Bounding the role of black carbon in the climate system: A scientific assessment. *Journal of Geophysical Research: Atmospheres*, **118 (11)**, 5380–5552.

Booth, B., N. Dunstone, P. Paul R. Halloran, T. Andrews, and N. Bellouin, 2012: Aerosols implicated as a prime driver of twentieth-century North Atlantic climate variability. *Nature*, **484**, 228–232.

Boucher, O., and M. Reddy, 2008: Climate trade-off between black carbon and carbon dioxide emissions. *Energy Policy*, **36**, 193–200.

Brönnimann, S., 2009: Early twentieth-century warming. *Nature Geoscience Correspondance*, **2**, 735–736.

Cai, W., and Coauthors, 2015: ENSO and greenhouse warming. *Nature Climate Change*, **5**, 849–859.

Cane, M., A. Clement, L. Murphy, and K. Bellomo, 2017: Low-Pass Filtering, Heat Flux, and Atlantic Multidecadal Variability. *Journal of Climate*, **30**, 7529–7553.

Carslaw, K., and Coauthors, 2013: Large contribution of natural aerosols to uncertainty in indirect forcing. *Nature*, **503 (7474)**, 67–71.

Cheng, L., K. Trenberth, M. Palmer, J. Zhu, and J. Abraham, 2016: Observed and simulated full-depth ocean heat-content changes for 1970-2005. *Ocean Science*, **12**, 925–935.

Chung, E.-S., and B. Soden, 2017: Hemispheric climate shifts driven by anthropogenic aerosol-cloud interactions. *Nature Geoscience*, **10**, 566–572, doi:10.1038/ngeo2988.

Chylek, P., C. K. Folland, G. Lesins, M. K. Dubey, and M. Wang, 2009: Arctic air temperature change amplification and the Atlantic Multidecadal Oscillation. *Geophysical Research Letters*, **36 (14)**, L14 801.

Chylek, P., J. Klett, G. Lesins, M. Dubey, and N. Hengartner, 2014: The Atlantic Multidecadal Oscillation as a dominant factor of oceanic influence on climate. *Geophysical Research Letters*, **41 (5)**, 1689–1697.

Clement, A., K. Bellomo, L. Murphy, M. Cane, T. Mauritsen, G. Rädel, and B. Stevens, 2015: The Atlantic Multidecadal Oscillation without a role for ocean circulation. *Science*, **350 (6258)**, 320–324.

Clement, A., M. Cane, L. Murphy, K. Bellomo, T. Mauritsen, and B. Stevens, 2016: Response to Comment on "The Atlantic Multidecadal Oscillation without a role for ocean circulation". *Science*, **352 (6293)**, 1527b.

Cohen, J. L., J. C. Furtado, M. Barlow, V. A. Alexeev, and J. E. Cherry, 2012: Asymmetric seasonal temperature trends. *Geophysical Research Letters*, **39 (4)**, L04 705.

Cohen, J. L., and Coauthors, 2014: Recent Arctic ampli cation and extreme mid-latitude weather. *Nature Geoscience*, **7**, 627–637.

Cowtan, K., R. Rohde, and Z. Hausfather, 2017: Estimating biases in Sea Surface Temperature records using coastal weather stations. *Quarterly Journal of the Royal Meteorological Society*, **in review**.

Cowtan, K., and R. Way, 2014: Coverage bias in the HadCRUT4 temperature series and its impact on recent temperature trends. *Quarterly Journal of the Royal Meteorological Society*, **140 (683)**, 1935–1944.

Cowtan, K., and Coauthors, 2015: Robust comparison of climate models with observations using blended land air and ocean sea surface temperatures. *Geophysical Research Letters*, **42 (15)**, 6526–6534.

Crowley, T., and M. Unterman, 2013: Technical details concerning development of a 1200 yr proxy index for global volcanism. *Earth System Science Data*, **5**, 187–197, doi:10.5194/essd-5-187-2013.

Crowley, T., G. Zielinski, B. Vinther, R. Udisti, K. Kreutz, J. Cole-Dai, and E. Castellano, 2008: Volcanism and the little ice age. *PAGES News*, **16 (2)**, 22–23.

Dallafior, T., D. Folini, R. Knutti, and M. Wild, 2016: Mixed-layer ocean responses to anthropogenic aerosol dimming from 1870 to 2000. *Journal of Geophysical Research: Atmospheres*, **121**, 49–66, doi:10.1002/2015JD024070.

Davis, L.L.B., D.W.J. Thompson, J.J.. Kennedy, and E.C. Kent, 2019: The importance of unresolved biases in 20th century sea-surface temperature observations. *Bulletin of the American Meteorological Society*, **99 (12)**, doi:10.1175/BAMS-D-18-0104.1.

de Boisséson, E., M. Balmaseda, S. Abdalla, E. Källén, and P. Janssen, 2014: How robust is the recent strengthening of the Tropical Pacific trade winds? *Geophysical Research Letters*, **41**, 4398–4405.

Delworth, T., and M. Mann, 2000: Observed and simulated multidecadal variability in the Northern Hemisphere. *Climate Dynamics*, **16**, 661–676.

Deser, C., R. Guo, and F. Lehner, 2017: The relative contributions of tropical Pacific sea surface temperatures and atmospheric internal variability to the recent global warming hiatus. *Geophysical Research Letters*, **44 (15)**, 7945–7954.

Deser, C., and Coauthors, 2012: ENSO and pacific decadal variability in the community climate system model version 4. *Journal of Climate*, **25 (8)**, 2622–2651.

Dewitte, S., and S. Nevens, 2016: The total solar irradiance climate data record. *The Astrophysical Journal*, **830 (25)**, 1–5.

DiNezio, P., B. Kirtman, A. Clement, S.-K. Lee, G. Vecchi, and A. Wittenberg, 2012: Mean Climate Controls on the Simulated Response of ENSO to Increasing Greenhouse Gases. *Journal of Climate*, **25**, 7399–7420.

Ding, Y., J. Carton, G. Chepurin, G. Stenchikov, A. Robock, L. Sentman, and J. Krasting, 2014: Ocean response to volcanic eruptions in Coupled Model Intercomparison Project 5 simulations. *Journal of Geophysical Research: Oceans*, **119**, 1–16.

Dong, L., and M. McPhaden, 2017: The role of external forcing and internal variability in regulating global mean surface temperatures on decadal timescales. *Environmental Research Letters*, **12**, 034 011.

Dong, L., T. Zhou, and X. Chen, 2014: Changes of Pacific decadal variability in the twentieth century driven by internal variability, greenhouse gases, and aerosols. *Geophysical Research Letters*, **41**, 8570–8577.

Donlon, C. J., M. Martin, J. Stark, J. Roberts-Jones, E. Fiedler, and W. Wimmer, 2012: The Operational Sea Surface Temperature and Sea Ice Analysis (OSTIA) system. *Remote Sensing of the Environment*, **116**, 140–158, doi:10.1016/j.rse.2010.10.017.

Duchez, A., and Coauthors, 2016: Drivers of exceptionally cold North Atlantic Ocean temperatures and their link to the 2015 European heat wave. *Environmental Research Letters*, **11**, 074 004.

Dumitrescu, A., C. Gueymard, and V. Badescu, 2017: Reconstruction of historical aerosol optical depth time series over Romania during summertime. *International Journal of Climatology*, **37**, in press.

Emile-Geay, J., R. Seager, M. Cane, E. Cook, and G. Haug, 2008: Volcanoes and ENSO over the Past Millennium. *Journal of Climate*, **21**, 3134–3148.

England, M., and Coauthors, 2014: Recent intensification of wind-driven circulation in the Pacific and the ongoing warming hiatus. *Nature Climate Change*, **4**, 222–227.

Etminan, M., G. Myhre, E. Highwood, and K. Shine, 2016: Radiative forcing of carbon dioxide, methane, and nitrous oxide: A significant revision of the methane radiative forcing. *Geophysical Research Letters*, **43**, 12,614–12,623.

Flato, G., and Coauthors, 2013: *Evaluation of Climate Models. In: Climate Change 2013: The Physical Science Basis. Contribution of Working Group I to the Fifth Assessment Report of the Intergovernmental Panel on Climate Change*. Cambridge University Press, Cambridge, United Kingdom and New York, NY, USA.

Folland, C., O. Boucher, and D. Colman, A.and Parker, 2018: Causes of irregularities in trends of global mean surface temperature since the late 19th century. *Science Advances*, **4 (6)**, eaao5297.

Forest, C., 2018: Inferred Net Aerosol Forcing Based on Historical Climate Changes: a Review. *Current Climate Change Reports*, **4 (1)**, 11–22, doi:10.1007/s40641-018-0085-2.

Forster, P., T. Andrews, P. Good, J. Gregory, L. Jackson, and M. Zelinka, 2013: Evaluating adjusted forcing and model spread for historical and future scenarios in the CMIP5 generation of climate models. *Journal of Geophysical Reseach*, **118**, 1–12.

Foster, G., and S. Rahmstorf, 2011: Global temperature evolution 1979-2010. *Environmental Research Letters*, **6**, 044 022.

Francis, J., 2017: Why Are Arctic Linkages to Extreme Weather Still Up in the Air? *Bulletin of the American Meteorological Society*, **98**, in press.

Frankignoul, C., G. Gastineau, and Y.-O. Kwon, 2017: Estimation of the SST response to anthropogenic and external forcing, and its impact on the Atlantic Multidecadal Oscillation and the Pacific Decadal Oscillation. *Journal of Climate*, **30**, in press.

Geoffroy, O., D. Saint-Martin, G. Bellon, A. Voldoire, D. Olivie, and S. Tyteca, 2013a: Transient Climate Response in a Two-Layer Energy-Balance Model. Part II: Representation of the Efficacy of Deep-Ocean Heat Uptake and Validation for CMIP5 AOGCMs. *Journal of Climate*, **26**, 1859–1876.

Geoffroy, O., D. Saint-Martin, D. Olivie, A. Voldoire, G. Bellon, and S. Tyteca, 2013b: Transient Climate Response in a Two-Layer Energy-Balance Model. Part I: Analytical Solution and Parameter Calibration Using CMIP5 AOGCM Experiments. *Journal of Climate*, **26**, 1841–1857.

Gregory, J., T. Andrews, and P. Good, 2015: The inconstancy of the transient climate response parameter under increasing CO2. *Philosophical Transactions of the Royal Society A*, **373 (2054)**, 20140 417.

Guan, B., and S. Nigam, 2009: Analysis of Atlantic SST Variability Factoring Interbasin Links and the Secular Trend: Clarified Structure of the Atlantic Multidecadal Oscillation. *Journal of Climate*, **22**, 4228–4240.

Hansen, J., R. Ruedy, M. Sato, and K. Lo, 2010: Global surface temperature change. *Reviews of Geophysics*, **48 (RG4004)**, 1–29.

Hansen, J., and Coauthors, 2016: Ice melt, sea level rise and superstorms: evidence from pale-oclimate data, climate modeling, and modern observations that 2C global warming could be dangerous. *Atmospheric Chemistry and Physics*, **16**, 3761–3812.

Hausfather, Z., K. Cowtan, D. Clarke, P. Jacobs, M. Richardson, and R. Rohde, 2017: Assessing recent warming using instrumentally homogeneous sea surface temperature records. *Science Advances*, **3 (1)**, e1601 207.

Haustein, K., M. Allen, P. Forster, F. Otto, D. Mitchell, H. D. Matthews, and D. Frame, 2017: A robust real-time Global Warming Index. *Nature Scientific Reports*, **7 (15417)**, 1–6.

Hay, S., P. Kushner, R. Blackport, and K. McCusker, 2018: On the relative robustness of the climate response to high-latitude and low-latitude warming. *Geophysical Research Letters*, **accepted**.

Hegerl, G., S. Brönnimann, A. Schurer, and T. Cowan, 2018: The early 20th century warming: Anomalies, causes,and consequences. *WIREs Climate Change*, **2018;e522**, 1–20, doi:10.1002/wcc.522.

Henley, B., 2017: Pacific decadal climate variability: Indices, patterns and tropical-extratropical interactions. *Global and Planetary Change*, **155**, 42–55.

Hetzinger, S., M. Pfeiffer, W.-C. Dullo, N. Keenlyside, M. Latif, and J. Zinke, 2008: Caribbean coral tracks Atlantic Multidecadal Oscillation and past hurricane activity. *Geology*, **36 (1)**, 11–14.

Hirahara, S., M. Ishii, and Y. Fukuda, 2014: Centennial-Scale Sea Surface Temperature Analysis and Its Uncertainty. *Journal of Climate*, **27**, 57–75.

Hodgkins, G., and D. Wilson, 2017: Climate-driven variability in the occurrence of major floods across North America and Europe. *Journal of Hydrology*, **552**, 704–717.

Hoesly, R., and Coauthors, 2017: Historical (1750-2014) anthropogenic emissions of reactive gases and aerosols from the Community Emission Data System (CEDS). *Geoscientific Model Development*, **11**, 369–408.

Huang, B., W. Angel, and T. Boyer, 2018: Evaluating SST Analyses with Independent Ocean Profile Observations. *Journal of Climate*, doi:10.1175/JCLI-D-17-0824.1.

Huang, B., and Coauthors, 2017: Extended Reconstructed Sea Surface Temperature version 5 (ERSSTv5): Upgrades, Validations, and Intercomparisons. *Journal of Climate*, **30 (21)**, in press, doi:10.1175/JCLI-D-16-0836.1.

Huber, M., and R. Knutti, 2014: Natural variability, radiative forcing and climate response in the recent hiatus reconciled. *Nature Geoscience*, **7**, 651–656.

Hurrell, J. W., and C. Deser, 2009: North Atlantic climate variability: the role of the North Atlantic Oscillation. *Journal of Maritime Systems*, **78**, 28–41.

Huss, M., R. Hock, A. Bauder, and M. Funk, 2010: 100-year mass changes in the Swiss Alps linked to the Atlantic Multidecadal Oscillation. *Geophysical Research Letters*, **37 (10)**, L10 501.

Iwi, A., L. Hermanson, K. Haines, and R. Sutton, 2012: Mechanisms Linking Volcanic Aerosols to the Atlantic Meridional Overturning Circulation. *Journal of Climate*, **25**, 3039–3051.

Johannessen, O. M., and Coauthors, 2004: Arctic climate change: observed and modelled temperature and sea-ice variability. *Tellus A*, **56**, 328–341.

41

Jones, G., P. Stott, and N. Christidis, 2013: Attribution of observed historical near-surface temperature variations to anthropogenic and natural causes using CMIP5 simulations. *Journal of Geophysical Research: Atmospheres*, **118**, 4001–4024.

Jones, G., P. Stott, and J. Mitchell, 2016: Uncertainties in the attribution of greenhouse gas warming and implications for climate prediction. *Journal of Geophysical Research: Atmospheres*, **121 (12)**, 6969–6992.

Josey, S.A., M.F.. de Jong, M. Oltmanns, G.K. Moore, and R.A. Weller, 2019: Extreme Variability in Irminger Sea Winter Heat Loss Revealed by Ocean Observatories Initiative Mooring and the ERA5 Reanalysis. *Geophysical Research Letters*, **46**, 1–10.

Kajtar, J., A. Santoso, S. McGregor, M. England, and Z. Baillie, 2017: Model under-representation of decadal Pacific trade wind trends and its link to tropical Atlantic bias. *Climate Dynamics*, **49**, 1–14.

Karl, T., and Coauthors, 2015: Possible artifacts of data biases in the recent global surface warming hiatus. *Science*, **348 (6242)**, 1469–1472.

Kennedy, J., N. Rayner, S. Millington, and M. Saunby, 2017: The Met Office Hadley Centre sea ice and sea surface temperature data set, version 2: 2. Sea surface temperature analysis. *Journal of Geophysical Research: Atmospheres*, **in preparation**.

Kennedy, J., N. Rayner, R. Smith, M. Saunby, and P. D.E., 2011: Reassessing biases and other uncertainties in sea-surface temperature observations measured in situ since 1850: 2. Biases and homogenization. *Journal of Geophysical Reseach*, **116 (D14)**, D14 104.

Kent, E., and Coauthors, 2017: A Call for New Approaches to Quantifying Biases in Observations of Sea Surface Temperature. *Bulletin of the American Meteorological Society*, **98 (9)**, in press.

Klimont, Z., S. Smith, and J. Cofala, 2013: The last decade of global anthropogenic sulfur dioxide: 2000-2011 emissions. *Environmental Research Letters*, **8**, 014 003.

Knight, J., R. Allan, C. Folland, M. Vellinga, and M. Mann, 2005: A signature of persistent natural thermohaline circulation cycles in observed climate. *Geophysical Research Letters*, **32 (20)**, L20 708.

Knight, J., C. Folland, and A. Scaife, 2006: Climate impacts of the Atlantic Multidecadal Oscillation. *Geophysical Research Letters*, **33 (17)**, L17 706.

Knudsen, M., B. Jacobsen, M.-S. Seidenkrantz, and J. Olsen, 2014: Evidence for external forcing of the Atlantic Multidecadal Oscillation since termination of the Little Ice Age. *Nature Communications*, **5 (3323)**.

Knutson, T., F. Zeng, and A. Wittenberg, 2013: Multimodel Assessment of Regional Surface Temperature Trends: CMIP3 and CMIP5 Twentieth-Century Simulations. *Journal of Climate*, **26**, 8709–8743.

Knutti, R., M. Rugenstein, and G. Hegerl, 2017: Beyond equilibrium climate sensitivity. *Nature Geoscience*, **10**, 727–736.

Kohyama, T., and D. Hartmann, 2017: No Access Nonlinear ENSO Warming Suppression (NEWS). *Journal of Climate*, **30**, 4227–4251.

Kosaka, Y., and S.-P. Xie, 2013: Recent global-warming hiatus tied to equatorial Pacific surface cooling. *Nature*, **501**, 403–407.

Kunkel, D., H. Tost, and M. Lawrence, 2013: Aerosol pollution potential from major population centers. *Atmospheric Chemistry and Physics*, **13**, 4203–4222.

Le, T., 2017: ENSO response to external forcing in CMIP5 simulations of the last millennium. *Global and Planetary Change*, **148**, 105–112.

Lean, J., 2018: Observation-based detection and attribution of 21st century climate change. *WIREs Climate Change*, **9:e511**, 1–20.

Lean, J., and D. Rind, 2008: How natural and anthropogenic influences alter global and regional surface temperatures: 1889 to 2006. *Geophysical Research Letters*, **35 (L18701)**.

Levine, A., D. Frierson, and M. McPhaden, 2018: AMO forcing of Multidecadal Pacific ITCZ variability. *Journal of Climate*, **in press**, doi:10.1175/JCLI-D-17-0810.1.

Lewis, N., and J. Curry, 2015: The implications for climate sensitivity of AR5 forcing and heat uptake estimates. *Climate Dynamics*, **45 (3-4)**, 1009–1023.

Lewis, N., and J. Curry, 2018: The impact of recent forcing and ocean heat uptake data on estimates of climate sensitivity. *Journal of Climate*, **in press**, doi:10.1175/JCLI-D17-0667.1.

L'Heureux, M. L., S. Lee, and B. Lyon, 2013: Recent multidecadal strengthening of the Walker circulation across the tropical Pacific. *Nature Climate Change*, **3**, 571–576.

Li, S., and A. Jarvis, 2009: Long run surface temperature dynamics of an A?OGCM: the HadCM3 4xCO(2) forcing experiment revisited. *Climate Dynamics*, **33 (6)**, 817–825.

Loeb, N., H. Wang, A. Cheng, S. Kato, J. Fasullo, K.-M. Xu, and R. Allan, 2016: Observational constraints on atmospheric and oceanic cross-equatorial heat transports: revisiting the precipitation asymmetry problem in climate models. *Climate Dynamics*, **46**, 3239–3257, doi: 10.1007/s00382-015-2766-z.

Lohmann, U., 2017: Why does knowledge of past aerosol forcing matter for future climate change? *Journal of Geophysical Research: Atmospheres*, **22 (9)**, 5021–5023.

Ma, S., and T. Zhou, 2016: Robust Strengthening and Westward Shift of the Tropical Pacific Walker Circulation during 1979–2012: A Comparison of 7 Sets of Reanalysis Data and 26 CMIP5 Models. *Journal of Climate*, **29**, 3097–3118.

Mahlstein, I., G. Hegerl, and S. Solomon, 2012: Emerging local warming signals in observational data. *Geophysical Research Letters*, **39 (21)**, L21 711.

Manara, V., M. Brunetti, M. Maugeri, A. Sanchez-Lorenzo, A., and M. Wild, 2017: Sunshine duration and global radiation trends in Italy (1959-2013): To what extent do they agree? *Journal of Geophysical Research: Atmospheres*, **122 (8)**, 4312–4331.

Mann, M., B. Steinman, and S. Miller, 2014: On Forced Temperature Changes, Internal Variability and the AMO. *Geophysical Research Letters*, **41 (9)**, 3211–3219.

Marini, C., and C. Frankignoul, 2014: An attempt to deconstruct the Atlantic Multidecadal Oscillation. *Journal of Climate*, **43**, 607–625.

Marvel, K., R. Pincus, G. Schmidt, and R. Miller, 2018: Internal Variability and Disequilibrium Confound Estimates of Climate Sensitivity From Observations. *Geophysical Research Letters*, **45 (3)**, 1595–1601.

Marvel, K., G. Schmidt, R. Miller, and L. Nazarenko, 2016: Implications for climate sensitivity from the response to individual forcings. *Nature Climate Change*, **6**, 386–389.

Mauritsen, T., and R. Pincus, 2017: Committed warming inferred from observations. *Nature Climate Change*, **7**, 652–655.

McConnell, J., and R. Edwards, 2008: Coal burning leaves toxic heavy metal legacy in the Arctic. *Proceedings of the National Acadamy of Science of USA*, **105 (34)**, 12,140–12,144.

McConnell, J., and Coauthors, 2007: 20th-Century Industrial Black Carbon Emissions Altered Arctic Climate Forcing. *Science*, **317**, 1381–1384.

McGregor, H., and Coauthors, 2015: Robust global ocean cooling trend for the pre-industrial Common Era. *Nature Geoscience*, **8**, 671–677.

McGregor, S., A. Timmermann, M. Stuecker, M. England, M. Merrifield, F.-F. Jin, and Y. Chikamoto, 2014: Recent Walker circulation strengthening and Pacific cooling amplified by Atlantic warming. *Nature Climate Change*, **4**, 888–892.

Medhaug, I., M. Stolpe, E. Fischer, and R. Knutti, 2017: Reconciling controversies about the 'global warming hiatus'. *Nature*, **545**, 41–47.

Meinshausen, M., and Coauthors, 2011: The RCP greenhouse gas concentrations and their extensions from 1765 to 2300. *Climatic Change*, **109**, 213–241, doi:10.1007/s10584-011-0156-z.

Meinshausen, M., and Coauthors, 2017: Historical greenhouse gas concentrations for climate modelling (CMIP6) . *Geoscientific Model Development*, **10**, 2057–2116, doi:10.5194/gmd-10-2057-2017.

Menary, M., and R. Wood, 2018: An anatomy of the projected North Atlantic warming hole in CMIP5 models. *Climate Dynamics*, **50 (7-8)**, 3063–3080.

Millar, R., Z. Nicholls, P. Friedlingstein, and A. M.R., 2017: A modified impulse-response representation of the global near-surface air temperature and atmospheric concentration response to carbon dioxide emissions. *Atmosheric Chemistry and Physics*, **17**, 7213–7228.

Morice, C., J. Kennedy, N. Rayner, and P. Jones, 2012: Quantifying uncertainties in global and regional temperature change using an ensemble of observational estimates: The HadCRUT4 data set. *Journal of Geophysical Reseach*, **117 (D8)**, D08 101.

Murphy, L., K. Bellomo, M. Cane, and A. Clement, 2017: The role of historical forcings in simulating the observed Atlantic multidecadal oscillation. *Geophysical Research Letters*, **44 (5)**, 2472–2480.

Myhre, G., and B. Samset, 2015: Standard climate models radiation codes underestimate black carbon radiative forcing. *Atmosheric Chemistry and Physics*, **15**, 2883–2888.

Myhre, G., and Coauthors, 2013: *Anthropogenic and Natural Radiative Forcing.* Climate Change 2013: The Physical Science Basis. Contribution of Working Group I to the Fifth Assessment Report of the Intergovernmental Panel on Climate Change, Cambridge University Press, Cambridge, United Kingdom and New York, NY, USA.

Myhre, G., and Coauthors, 2017: Multi-model simulations of aerosol and ozone radiative forcing due to anthropogenic emission changes during the period 1990-2015. *Atmospheric Chemistry and Physics*, **17**, 2709–2720.

Nazarenko, L., D. Rind, K. Tsigaridis, A. Del Genio, M. Kelley, and N. Tausnev, 2017: Interactive nature of climate change and aerosol forcing. *Journal of Geophysical Research: Atmospheres*, **122 (6)**, 3457–3480.

Newman, M., and Coauthors, 2016: The Pacific Decadal Oscillation, Revisited. *Journal of Climate*, **29**, 4399–4427.

O'Reilly, C., M. Huber, T. Woollings, and L. Zanna, 2016: The signature of low-frequency oceanic forcing in the Atlantic Multidecadal Oscillation. *Geophysical Research Letters*, **43**, 2810–2818.

Otterå, O., M. Bentsen, H. Drange, and L. Suo, 2010: External forcing as a metronome for Atlantic multidecadal variability. *Nature Geoscience*, **3**, 688–694.

Otto, A., and Coauthors, 2013: Energy budget constraints on climate response. *Nature Geoscience Correspondance*, **6**, 415–416.

Otto, F., D. Frame, A. Otto, and M. Allen, 2015: Embracing uncertainty in climate change policy. *Nature Climate Change*, **5**, 917–920.

Overland, J., 2016: A difficult Arctic science issue: Midlatitude weather linkages. *Polar Science*, **10 (3)**, 210–216.

Pasini, A., U. Triacca, and A. Attanasio, 2016: Evidence for the role of the Atlantic multidecadal oscillation and the ocean heat uptake in hiatus prediction. *Theoretical and Applied Climatology*, **129 (3-4)**, 873–880.

Pausata, F., L. Chafik, R. Caballeroa, and D. Battisti, 2015: Impacts of high-latitude volcanic eruptions on ENSO and AMOC. *Proceedings of the National Acadamy of Science of USA*, **112 (45)**, 13,784–13,788.

Persad, G., and K. Caldeira, 2018: Divergent global-scale temperature effects from identical aerosols emitted in different regions. *Nature Communications*, **9 (3289)**, 1–9.

Piecuch, C., R. Ponte, C. Little, M. Buckley, and I. Fukumori, 2017: Mechanisms underlying recent decadal changes in subpolar North Atlantic Ocean heat content. *Journal of Geophysical Research: Oceans*, **122**, 7181–7197.

Pinto, J., M. Reyers, and U. Ulbrich, 2011: The variable link between PNA and NAO in observations and in multi-century CGCM simulations. *Climate Dynamics*, **36 (1-2)**, 337–354.

Proistosescu, C., and P. Huybers, 2017: Slow climate mode reconciles historical and model-based estimates of climate sensitivity. *Science Advances*, **3 (7)**, e1602 821.

Rahmstorf, S., J. Box, G. Feulner, M. Mann, A. Robinson, S. Rutherford, and E. Schaffernicht, 2015: Exceptional twentieth-century slowdown in Atlantic Ocean overturning circulation. *Nature Climate Change*, **5**, 475–480.

Rahmstorf, S., G. Foster, and N. Cahill, 2017: Global temperature evolution: recent trends and some pitfalls. *Environmental Research Letters*, **12**, 054 001.

Regayre, L., and Coauthors, 2014: Uncertainty in the magnitude of aerosol-cloud radiative forcing over recent decades. *Geophysical Research Letters*, **41**, 9040–9049.

Ribes, A., F. Zwiers, J.-M. Azaïs, and P. Naveau, 2017: A new statistical approach to climate change detection and attribution. *Climate Dynamics*, **48 (1-2)**, 367–386.

Richardson, M., K. Cowtan, E. Hawkins, and M. Stolpe, 2016: Reconciled climate response estimates from climate models and the energy budget of Earth. *Nature Climate Change*.

Roberts, C., and Coauthors, 2013: Atmosphere drives recent interannual variability of the Atlantic meridional overturning circulation at 26.5N. *Geophysical Research Letters*, **40**, 5164–5170.

Rohde, R., and Coauthors, 2012: A New Estimate of the Average Earth Surface Land Temperature Spanning 1753 to 2011. *Geoinformatics and Geostatistics: An Overview*, **1 (1)**, 1–7.

Rotstayn, L., M. Collier, D. Shindell, and O. Boucher, 2015: Why Does Aerosol Forcing Control Historical Global-Mean Surface Temperature Change in CMIP5 Models? *Journal of Climate*, **28**, 6608–6625.

Rypdal, K., 2012: Global temperature response to radiative forcing: Solar cycle versus volcanic eruptions. *Journal of Geophysical Reseach*, **117 (D6)**, D06 115.

Rypdal, K., 2018: The Life and Death of the Hiatus Consistently Explained. *Preprints*, doi:10.20944/preprints201805.0372.v1.

49

Santer, B., and Coauthors, 2014: Volcanic contribution to decadal changes in tropospheric temperature. *Nature Geoscience*, **7**, 185–189.

Sato, M., J. Hansen, M. McCormick, and J. Pollack, 1993: Stratospheric aerosol optical depth, 1850-1990. *Journal of Geophysical Research*, **98**, 22,987–22,994, doi:10.1029/93JD02553.

Scaife, A., and Coauthors, 2014: Skillful long-range prediction of European and North American winters. *Geophysical Research Letters*, **41 (7)**, 2514–2519.

Schmidt, A., and Coauthors, 2018: Volcanic radiative forcing from 1979-2015. *Geophysical Research Letters*, **in review**.

Schmidt, G., D. Shindell, and K. Tsigaridis, 2014: Reconciling warming trends. *Nature Geoscience*, **7**, 158–160.

Schulz, M., and Coauthors, 2012: Atmospheric Transport and Deposition of Mineral Dust to the Ocean: Implications for Research Needs. *Environmental Science and Technology*, **46**, 10,390–10,404.

Schurer, A., G. Hegerl, and S. Obrochta, 2015: Determining the likelihood of pauses and surges in global warming. *Geophysical Research Letters*, **42**, 5974–5982.

Schurer, A., S. Tett, and G. Hegerl, 2014: Small influence of solar variability on climate over the past millennium. *Nature Geoscience*, **7**, 104–108.

Serreze, M., and R. Barry, 2011: Processes and impacts of Arctic amplification: A research synthesis. *Global and Planetary Change*, **77**, 85–96.

Sévellec, F., A. Fedorov, and W. Liu, 2017: Arctic sea-ice decline weakens the Atlantic Meridional Overturning Circulation. *Nature Climate Change*, **7**, 604–610.

Shen, L., L. Mickley, E. Leibensperger, and M. Li, 2018: Strong dependence of U.S. summertime air quality on the decadal variability of Atlantic sea surface temperatures. *Geophysical Research Letters*, **44**, 12 527–12 535.

Shindell, D., 2014: Inhomogeneous forcing and transient climate sensitivity. *Nature Climate Change*, **4**, 274–277.

Shindell, D., and Coauthors, 2013: Radiative forcing in the ACCMIP historical and future climate simulations. *Atmosheric Chemistry and Physics*, **12**, 2939–2974.

Shiogama, H., T. Nagashima, T. Yokohata, S. Crooks, and T. Nozawa, 2006: Influence of volcanic activity and changes in solar irradiance on surface air temperatures in the early twentieth century. *Geophysical Research Letters*, **33 (9)**, L09 702.

Singh, H., G. Hakim, R. Tardif, J. Emile-Geay, and D. Noone, 2018: Insights into Atlantic multidecadal variability using the Last Millennium Reanalysis framework. *Climate of the Past*, **14**, 157–174.

Skeie, R., T. Berntsen, M. Aldrin, M. Holden, and G. Myhre, 2014: A lower and more constrained estimate of climate sensitivity using updated observations and detailed radiative forcing time series. *Earth System Dynamics*, **5**, 139–175.

Smith, S., J. van Ardenne, Z. Klimont, R. Andres, A. Volke, and S. Delgado Arias, 2011: Anthropogenic sulfur dioxide emissions: 1850-2005. *Atmosheric Chemistry and Physics*, **11**, 1101–1116.

Solomon, S., J. Daniel, R. Neely III, J. Vernier, E. Dutton, and L. Thomason, 2011: The Persistently Variable "Background" Stratospheric Aerosol Layer and Global Climate Change. *Science*, **333**, 866–870, doi:10.1126/science.1206027.

Stephens, G., M. Hakuba, M. Hawcroft, J. Haywood, A. Behrangi, J. Kay, and P. Webster, 2016: The Curious Nature of the Hemispheric Symmetry of the Earth's Water and Energy Balances. *Current Climate Change Reports*, **2**, 135–147, doi:10.1007/s40641-016-0043-9.

Stevens, B., 2015: Rethinking the Lower Bound on Aerosol Radiative Forcing. *Journal of Climate*, **28**, 4794–4819, doi:10.1175/JCLI-D-14-00656.1.

Stocker, T., and Coauthors, 2013: *Technical summary. In Climate Change 2013: The Physical Science Basis. Contribution of Working Group I to the Fifth Assessment Report of the Intergovernmental Panel on Climate Change.* Cambridge University Press, Cambridge, United Kingdom and New York, NY, USA.

Stolpe, M., I. Medhaug, and R. Knutti, 2017: Contribution of Atlantic and Pacific multidecadal variability to twentieth century temperature changes. *Journal of Climate*, **30**, in press.

Stott, P., S. Tett, G. Jones, M. Allen, J. Mitchell, and G. Jenkins, 2000: External Control of 20th Century Temperature by Natural and Anthropogenic Forcings. *Science*, **290**, 2133–2137.

Stuecker, M., F.-F. Jin, and A. Timmermann, 2015: El Niño-Southern Oscillation frequency cascade. *Proceedings of the National Acadamy of Science of USA*, **112 (44)**, 13,490–13,495.

Suckling, E., G. van Oldenborgh, J. Eden, and E. Hawkins, 2017: An empirical model for probabilistic decadal prediction: global attribution and regional hindcasts. *Climate Dynamics*, **48 (9-10)**, 3115–3138.

Suo, S., O. Otterå, M. Bentsen, Y. Gao, and O. Johannessen, 2013: External forcing of the early 20th century Arctic warming. *Tellus A*, **65 (1)**, 20 578.

Sutton, R., G. D. McCarthy, J. Robson, B. Sinha, A. Archibald, and L. Gray, 2017: Atlantic Multi-decadal Variability and the UK ACSIS programme. *Bulletin of the American Meteorological Society*, **98 (9)**, in press.

Swingedouw, D., J. Mignot, P. Ortega, M. Khodri, M. Menegoz, C. Cassou, and V. Hanquiez, 2017: Impact of explosive volcanic eruptions on the main climate variability modes. *Global and Planetary Change*, **150**, 24–45.

Takahashi, C., and M. Watanabe, 2016: Pacific trade winds accelerated by aerosol forcing over the past two decades. *Nature Climate Change*, **6**, 768–772.

Tang, Q., X. Zhang, X. Yang, and J. Francis, 2013: Cold winter extremes in northern continents linked to Arctic sea ice loss. *Environmental Research Letters*, **8**, 014 036.

Taylor, K., R. Stouffer, and G. Meehl, 2012: An Overview of CMIP5 and the experiment design. *Bulletin of American Meteorological Society*, **93**, 485–498.

Thompson, D., J. Cole, G. Shen, A. Tudhope, and G. Meehl, 2015: Early twentieth-century warming linked to tropical Pacific wind strength. *Nature Geoscience*, **8**, 117–121.

Ting, M., Y. Kushnir, R. Seager, and C. Li, 2009: Forced and Internal Twentieth-Century SST Trends in the North Atlantic. *Journal of Climate*, **22**, 1469–1481.

Titchner, H., and N. Rayner, 2014: The Met Office Hadley Centre sea ice and sea surface temperature data set, version 2: 1. Sea ice concentrations. *Journal of Geophysical Research: Atmospheres*, **119**, 2864–2889.

Trenberth, K., 1997: The definition of El Niño. *Bulletin of the American Meteorological Society*, **78**, 2771–2777.

Tung, K., and J. Zhou, 2013: Using data to attribute episodes of warming and cooling in instrumental records. *Proceedings of the National Academy of the Sciences of the USA*, **110 (6)**, 2058–2063.

Uno, I., and Coauthors, 2009: Asian dust transported one full circuit around the globe. *Nature Geoscience*, **2**, 557–560.

van Oldenborgh, G., L. te Raa, H. Dijkstra, and S. Philip, 2009: Frequency- or amplitude-dependent effects of the Atlantic meridional overturning on the tropical Pacific Ocean. *Ocean Science*, **5**, 293–301.

Vecchi, G., T. Delworth, and B. Booth, 2017: Climate Science: Origins of Atlantic decadal swings. *Nature*, **548**, 284–285.

Vernier, J.-P., and Coauthors, 2011: Major influence of tropical volcanic eruptions on the stratospheric aerosol layer during the last decade. *Geophysical Research Letters*, **38 (12)**, L12 807, doi:10.1029/2011GL047563.

Vincze, M., and I. Jánosi, 2011: Is the Atlantic Multidecadal Oscillation (AMO) a statistical phantom? *Nonlinear Processes in Geophysics*, **18**, 469–475.

Wang, K., and Coauthors, 2017: Continuously amplified warming in the Alaskan Arctic: Implications for estimating global warming hiatus. *Geophysical Research Letters*, **44 (17)**, 9029–9038.

Way, R., F. Oliva, and A. Viau, 2017: Underestimated warming of northern Canada in the Berkeley Earth temperature product. *International Journal of Climatology*, **37 (4)**, 1746–1757.

Wilcox, L., E. Highwood, and N. Dunstone, 2013: The influence of anthropogenic aerosol on multi-decadal variations of historical global climate. *Environmental Research Letters*, **8**, 024 033.

Wild, M., 2009: Global dimming and brightening: A review. *Journal of Geophysical Research*, **114 (D10)**, D00D16.

Wild, M., A. Ohmura, and K. Makowski, 2007: Impact of global dimming and brightening on global warming. *Geophysical Research Letters*, **34 (4)**, L04 702.

Williams, B., and Coauthors, 2017: North Pacific twentieth century decadal-scale variability is unique for the past 342 years. *Geophysical Research Letters*, **44 (8)**, 3761–3769.

Wilson, R., and D. Hathaway, 2006: On the Relation Between Sunspot Area and Sunspot Number. Tech. Rep. 214324, Marshall Space Flight Center, Marshall Space Flight Center, Alabama.

Wolter, K., and M. Timlin, 1998: Measuring the strength of ENSO events - how does 1997/98 rank? *Weather*, **53**, 315–324.

Wyatt, M., S. Kravtsov, and A. Tsonis, 2012: Atlantic Multidecadal Oscillation and Northern Hemisphere's climate variability. *Climate Dynamics*, **38**, 929–949.

Xiang, B., B. Wang, J. Li, M. Zhao, and J.-Y. Lee, 2014: Understanding the Anthropogenically Forced Change of Equatorial Pacific Trade Winds in Coupled Climate Models. *Journal of Climate*, **27**, 8510–8526.

Yan, X., R. Zhang, and T. Knutson, 2017: The role of Atlantic overturning circulation in the recent decline of Atlantic major hurricane frequency. *Nature Communications*, **8 (1695)**, 1–8, doi:10.1038/s41467-017-01377-8.

Yeager, S., and J. Robson, 2017: Recent Progress in Understanding and Predicting Atlantic Decadal Climate Variability. *Current Climate Change Reports*, **3 (2)**, 112–127.

Zhang, L., and C. Wang, 2013: Multidecadal North Atlantic sea surface temperature and Atlantic meridional overturning circulation variability in CMIP5 historical simulations. *Journal of Geophysical Research: Oceans*, **118**, 1–20.

Zhang, R., 2017: On the persistence and coherence of subpolar sea surface temperature and salinity anomalies associated with the Atlantic multidecadal variability. *Geophysical Research Letters*, **44 (15)**, 7865–7875.

Zhang, R., R. Sutton, G. Danabasoglu, T. Delworth, W. Kim, J. Robson, and S. Yeager, 2016: Comment on "The Atlantic Multidecadal Oscillation without a role for ocean circulation". *Science*, **352 (6293)**, 1527a.

Zhang, R., and Coauthors, 2013: Have Aerosols Caused the Observed Atlantic Multidecadal Variability? *Journal of the Atmosheric Sciences*, **70**, 1135–1144.

Zhang, W., G. Vecchi, H. Murakami, G. Villarini, T. Delworth, X. Yang, and L. Jia, 2018: Dominant Role of Atlantic Multidecadal Oscillation in the Recent Decadal Changes in Western North Pacific Tropical Cyclone Activity. *Geophysical Research Letters*, **45 (1)**, 354–362.

57

Global Radiative Forcing Components (1730-2017)

a

GHG Forcing (AR5 updated) ... used here
GISS WMGHG Forcing
Aerosol Effective Forcing (CEDS) ... used here
Anthropogenic Aerosols (AR5)
Crowley12/Schmidt Eruptions ... used here
Volcanic Aerosols (AR5)
Solar with ozone UV effects ... used here
Solar Forcing (AR5)

Laki, SW Pacific, Tambora, Cosiguina, Shiveluch, Krakatoa, Santa Maria, Katmal, Agung, El Chichon, Pinatubo

Aerosol Forcing Contributions (based on CEDS emissions)

b

BC global
BC on Arctic snow
SO2 global
OC global
NH3 global
Indirect forcing
Global forcing
Effective forcing

Aerosol Effective Radiative Forcing Distribution

c

ERF Global
ERF NH
ERF SH
ERF Land
ERF Ocean
RF Global
RF NH
RF SH
RF Land
RF Ocean

Scaled Coastal HadISST2 anomalies 1850-2016 (baseline 1981-2010)

d

ERSSTv4 60N-60S
HadISST2/OSTIA 60N-60S
BerkeleyEarth Coastal 60N-60S (scaling factor = 0.46)
GISS Coastal 60N-60S (scaling factor = 0.46)
HadISST2/OSTIA Coastal 60N-60S (scaling factor = 0.70)
ERSSTv4 Coastal 60N-60S (scaling factor = 0.70)

Scaled Coastal ERSSTv4 anomalies 1850-2016 (baseline 1981-2010)

e

ERSSTv4 60N-60S
HadISST2/OSTIA 60N-60S
BerkeleyEarth Coastal 60N-60S (scaling factor = 0.46)
GISS Coastal 60N-60S (scaling factor = 0.46)
HadISST2/OSTIA Coastal 60N-60S (scaling factor = 0.70)
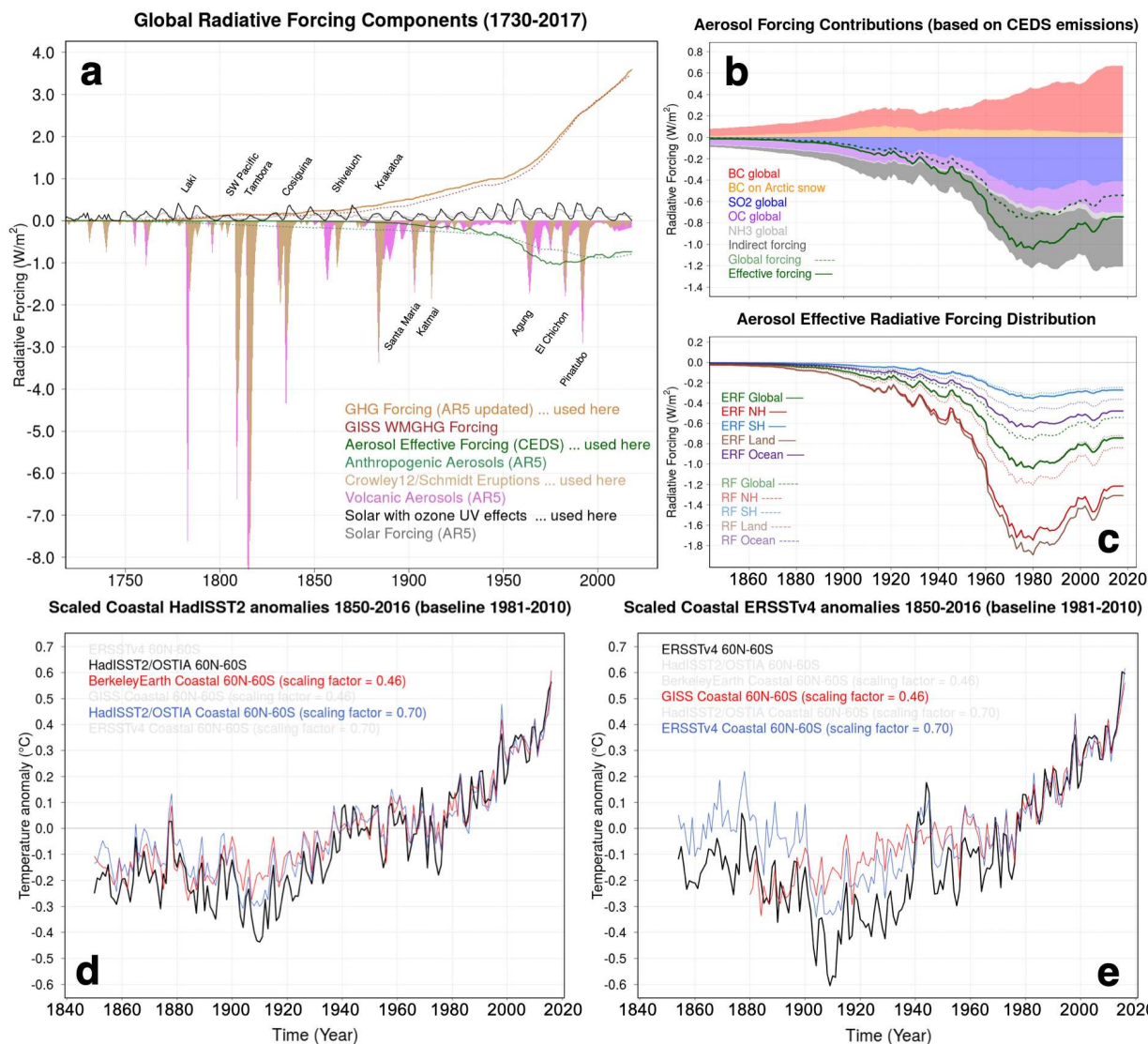ERSSTv4 Coastal 60N-60S (scaling factor = 0.70)

FIG. 1. Global radiative forcing components used in our study (a), decomposition of the four AER components including indirect aerosol effects (b), and spatial decomposition of the effective and non-effective AER (c). Scaled coastal HadOST (blue) and coastal BE anomalies (red) in comparison with 60N-60S HadOST (black) in (d) and the same for coastal ERSSTv4, coastal GISTEMP and 60N-60S ERSSTv4 in (e).

59

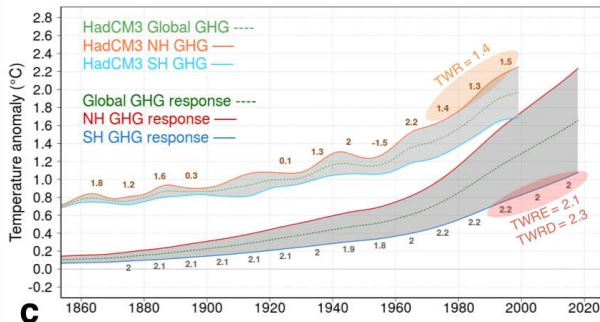**a** Hemispheric warming contributions: Model vs Observation
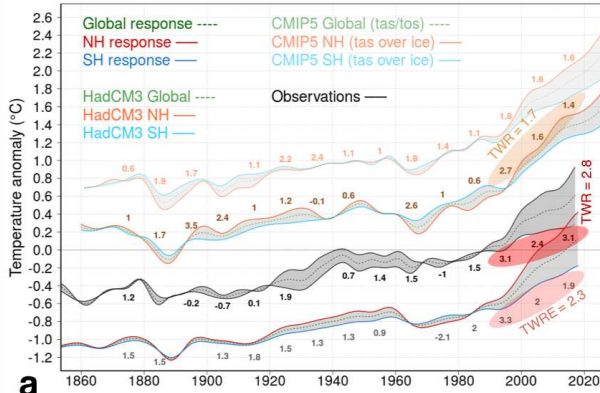
b Land/Ocean warming contributions: Model vs Observation
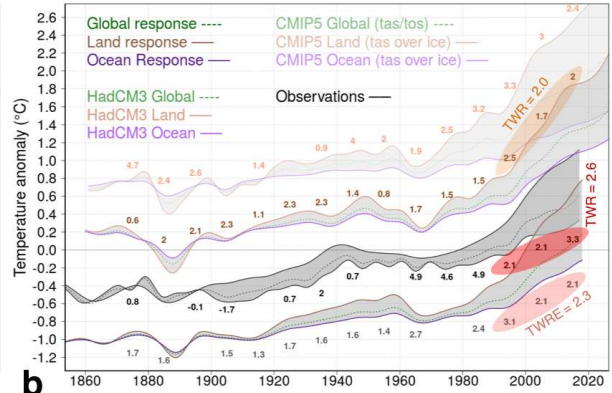
c GreenhouseGas-Only Forcing: Hemispheric Response Ratio

d GreenhouseGas-Only Forcing: Land/Ocean Response Ratio
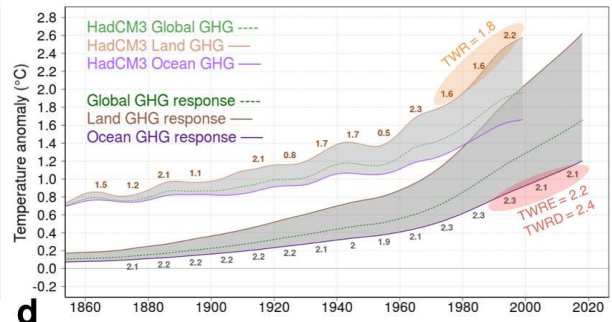
e Aerosol-Only Forcing: Hemispheric Response Ratio

f Aerosol-Only Forcing: Land/Ocean Response Ratio
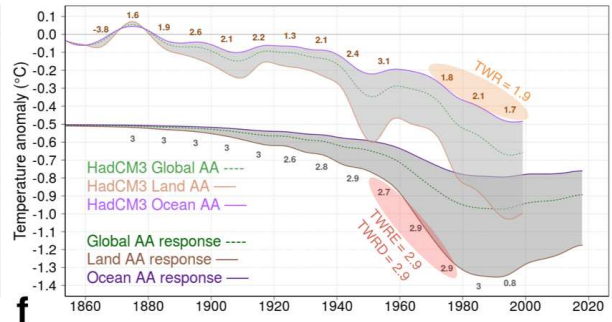
g Volcanic-Only Forcing: Hemispheric Response Ratio
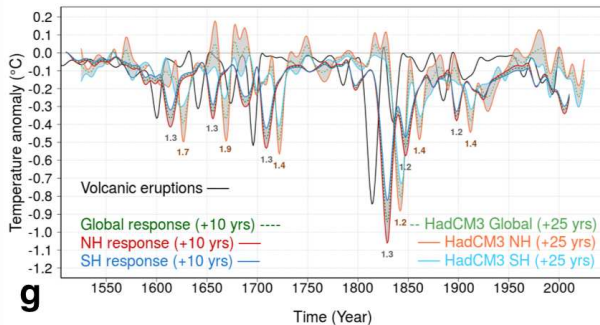
h Volcanic-Only Forcing: Land/Ocean Response Ratio
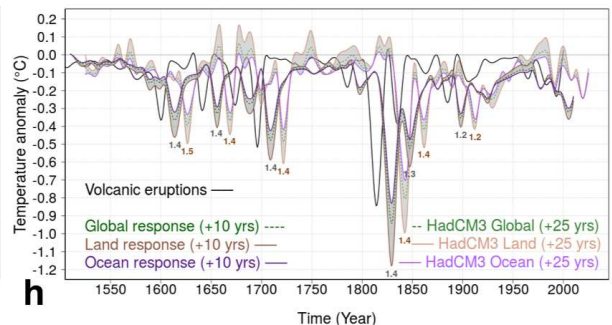
TWR = Transient Warming Ratio	**GHG-Only:** NHem/SHem = 1.4 x (2.8 / 1.7) = 2.3	**Land/Ocean** = 1.8 x (2.6 / 2.0) = 2.4
TWRE = Estimated Model TWR	**AER-Only:** NHem/SHem = 2.1 x (2.8 / 1.7) = 3.5*	**Land/Ocean** = 1.9 x (2.6 / 2.0) = 2.4**
TWRD = Diagnosed Model TWR	**VOL-Only:** NHem/SHem (fast) = 1.3 x 1.0 = 1.3	**Land/Ocean** (fast) = 1.4 x 1.0 = 1.4

60

FIG. 2. Transient Warming Ratios (TWR) to estimate the TCR adjustment factors for WMGHGs, AER and VOL for NHem/SHem (lhs) and Land/Ocean (rhs). *Allforcing* warming contributions in CMIP5, HadCM3, HadOST and the response model (a, b). WMGHG only (c, d), AER only (e, f) and VOL only (g, h) contributions in HadCM3 and the response model. Modelled VOL (negative) temperature response is shifted by +10 and +25 years merely for better readability. The timeline of volcanic eruptions (scaled radiative forcing) is shown in black (g, h). All data are low-pass filtered to remove interannual variability. The boxes at the bottom show the inferred (diagnosed) warming ratios (TWRD) for WMGHG and AER using the product of the ratios of observed (red) and modelled (orange) *allforcing* TWRs (a, b), multiplied by the modelled TWRs (orange) for WMGHG (c, d) and AER (e, f). The estimated warming ratios (TWRE) refer to the simulated response model TWR using TWRD. Both values are given in light purple. Only the 30 year period of strongest differential warming is used for the central TWR estimates. VOL TWR is only a function of the fast response.

61

Global TCR
- **GHG:** updated AR5 ……...… *1.6 K… example using best estimate*
- **AER:** CEDS emissions …… *2.2 K = TCR$_{GHG}$ x **AER ERF**/**AER RF***
- **VOL:** Crowley/Schmidt …… *1.6 K = TCR$_{GHG}$*

NHem/SHem* TCR
- **GHG:** *2.23/0.97 K …TWRD = 2.3 … HadCM3 GHG warming ratio*
- **AER:** *2.50/1.90 K …TWRD = 5.1 … HadCM3 **AER est.** warming ratio*
- **VOL:** *1.80/1.40 K …TWRD = 1.3 … HadCM3 **VOL fast** warming ratio*

Land/Ocean** TCR
- **GHG:** *2.65/1.11 K … TWRD = 2.4 … HadCM3 GHG warming ratio*
- **AER:** *2.70/1.95 K … TWRD = 2.9 … HadCM3 **AER est.** warming ratio*
- **VOL:** *2.00/1.40 K … TWRD = 1.4 … HadCM3 **VOL fast** warming ratio*

- ***Fast response time:*** *…………..…….. 8 yrs … Boucher and Reddy 2008*
- ***Slow response time:*** *……………. 320 yrs … Geoffroy et al. 2013b*
- ***Equilibrium Sensitivity (ECS):*** *…. 3.0 K …… best estimate with range of 2.0-4.0 K*
- ***Transient Response (TCR):*** *…….. 1.6 K …… best estimate with range of 1.1-2.1 K*
- ***TCR/ECS ratio:*** *………………..... 0.53 …… based on CMIP5 model mean*

- ***AER ERF:*** *………… Forest 2018; revised net effective aerosol forcing (0.75 W/m²)*
- ***AER RF:*** *…………… AR5 Ch.8; individual aerosol forcing components (0.55 W/m²)*
- ***AER estimated:*** *…. minor tuning of model deduced warming ratio (= 3.5*/ = 2.4**)*
  scaled w/ coupling factor to balance the sum (= 3.9*/ = 2.1**)
- ***VOL fast:*** *…………... direct model estimate (derived from fast forcing regime only)*

* **NHem/SHem** *area weighting factor = 0.50/0.50 (* for NHem/SHem) (* for NHem/SHem = 1.47/0.38)*
** **Land/Ocean** *area weighting factor = 0.32/0.68 (** for Land/Ocean) (** for Land/Ocean = 1.46/0.70)*
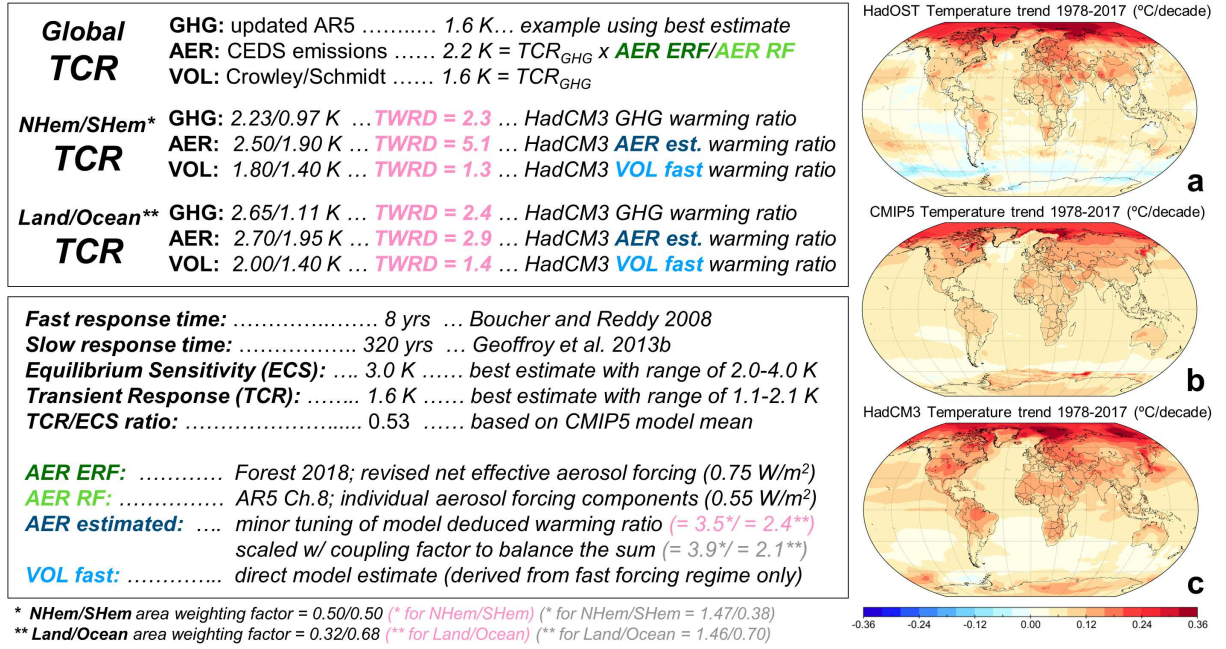
FIG. 3. Summary panel for all the necessary response model parameter, including their justification. Global, hemispheric and Land/Ocean TCR scaling factors for WMGHGs, anthropogenic aerosols (AER) and volcanic eruptions (VOL) based on the findings shown in Fig. 1 (top box). Forcing response time estimates and sensitivities used in this analysis are provided, including their source (bottom box). Colour codes for better readability. The pink labels in the lower box refer to the original AER-TWRD. In grey the associated coupling factors. Surface temperature trends in HadOST (a), CMIP5 (b) and HadCM3 (c) from 1978-2017.
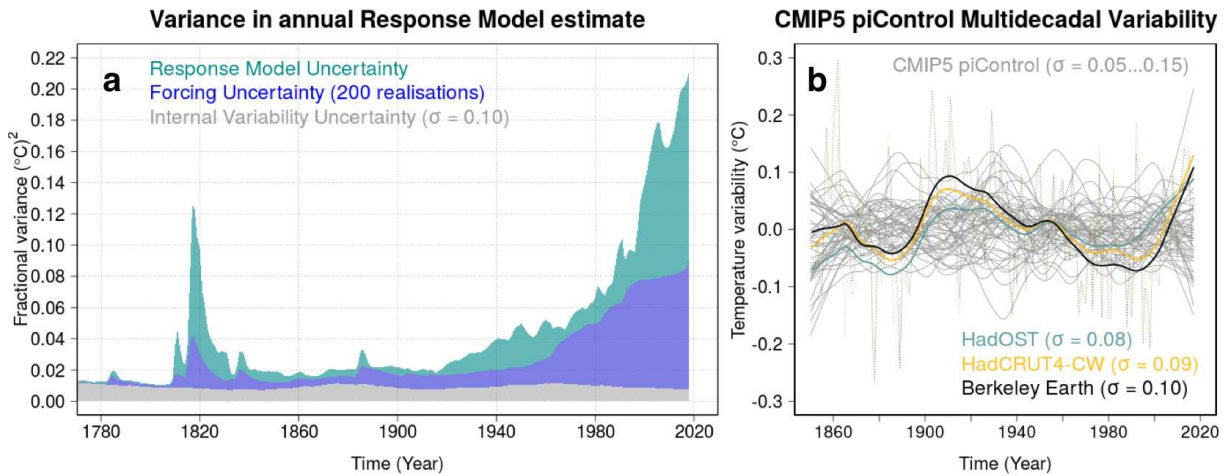
FIG. 4. Fractional variance (square of the model error) for impulse response model uncertainty (green), total radiative forcing uncertainty (blue) and internal variability uncertainty (grey) in (a). The 1σ (32-68th percentiles) range is shown. We note that internal variability is no response model uncertainty in a strict sense as it is added post-hoc (i.e. onto the calculated temperature). The peaks in the response model uncertainty coincide with volcanic eruptions (e.g. Tambora in 1816) eruption. The Internal variability from selected CMIP5 piControl runs is contrasted with the unforced residuals from the GMST datasets used in this study (b). Observed and modelled timeseries are low-pass filtered with a 30 year smoothing radius. The standard error is provided in brackets.

63

Impulse Response Model vs ENSO/MEI (1850-2017)
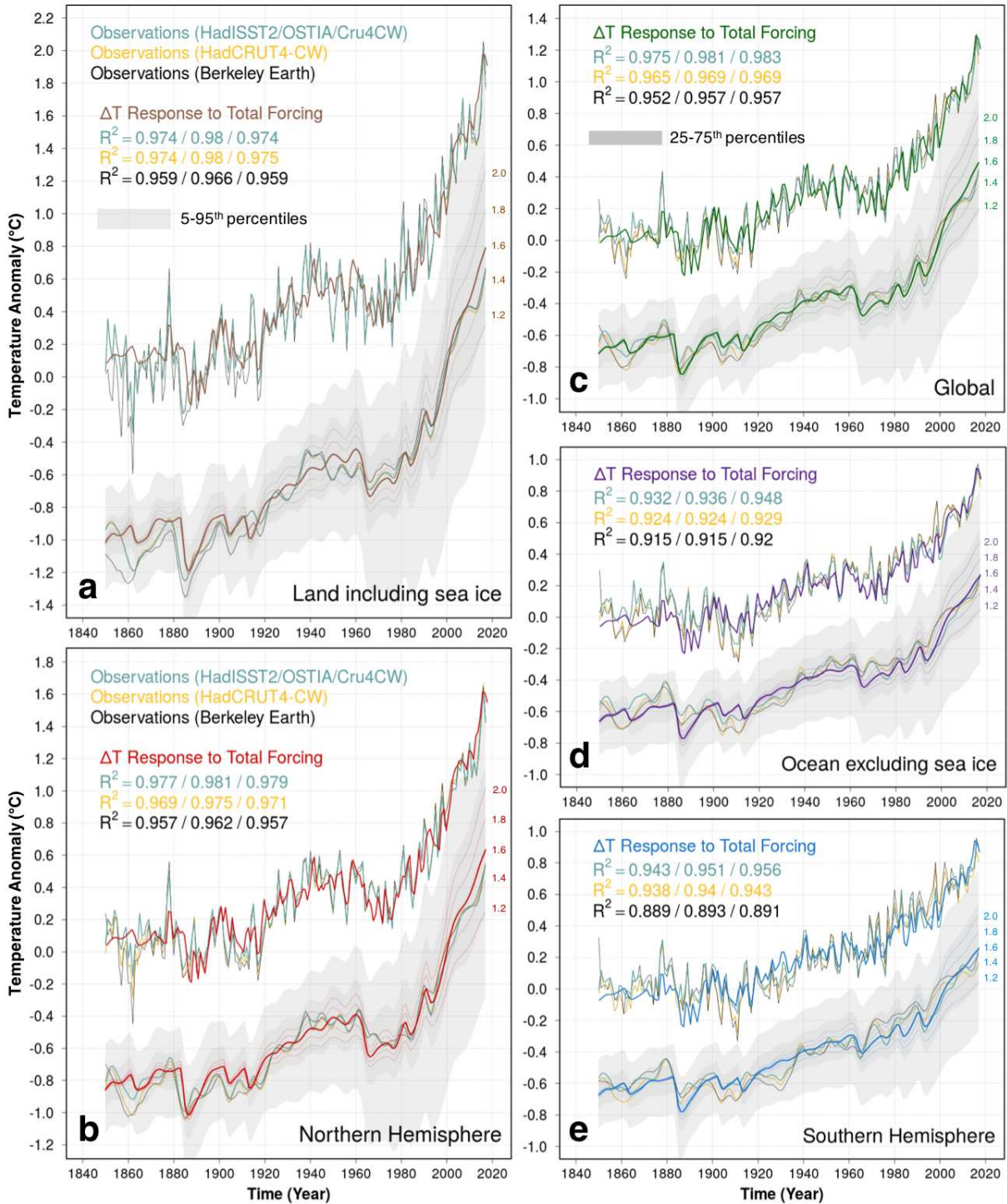
64

₁₂₉₇ FIG. 5. Illustration of the ENSO influence on our results. In the upper graph in each panel, the observations

₁₂₉₈ are plotted against the response after adding MEI variability to the time series. The lower graph shows the

₁₂₉₉ raw impulse response model results against the ENSO-corrected suite of observational data. Land (including

₁₃₀₀ sea ice grid points) is shown on the upper left (brown), NHem on the lower left (red), GMST on the upper

₁₃₀₁ right (green), Ocean (excluding sea ice grid points) in the centre right (purple), and SHem on the lower right

₁₃₀₂ (blue). Observations from the HadOST composite (pale grey), Cru4CW (yellow), and BE (black) are shown.

₁₃₀₃ Explained variances (R^2) are given for non-ENSO corrected, model-adjusted (MEI), and observation-adjusted

₁₃₀₄ (MEI) (Foster and Rahmstorf 2011) low-pass-filtered correlations. The WWII correction factors are applied to

₁₃₀₅ both instrumental temperature timeseries in each panel (except Land). TCR values associated with alternative

₁₃₀₆ response model results are provided on the right of each panel (1.2-2.0K).

Evolution of the Impulse Response Model
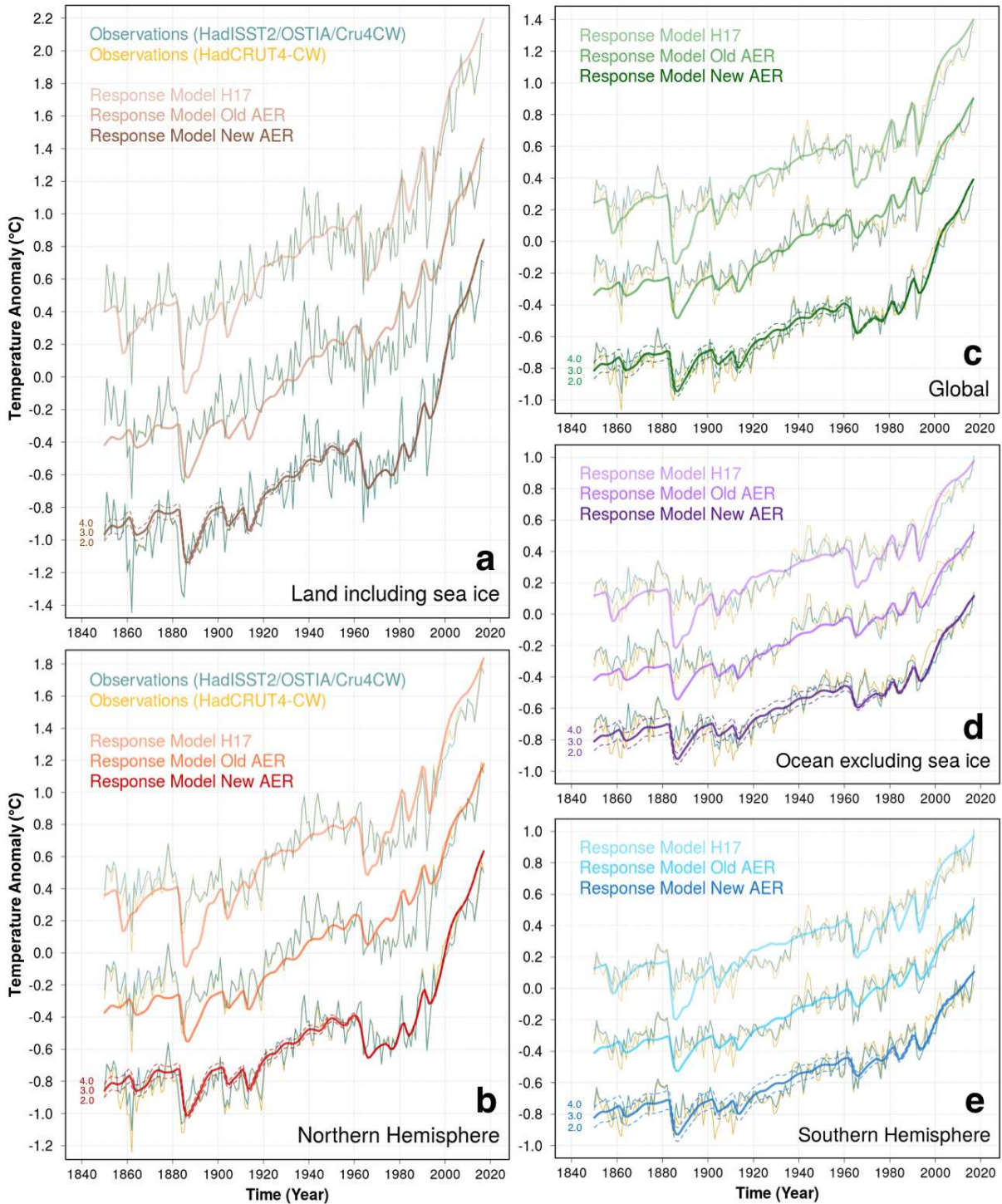
FIG. 6. Evolution of the response model from forcing and response times as applied in Haustein et al. (2017) (H17), with AER as used in CMIP5 (old AER) and the current version using CEDS AER (new AER). Note that the WWII bias correction is only applied in case of new AER in order to illustrate the impact (no change in Land only). The results are shown for Land (a), NHem (b), Global (c), Ocean (d) and SHem (e). The two dashed lines in the lower graph of each panel indicate the variability of the result as a function of the ECS value applied in the response model. The default value of 3.0K corresponds with our central estimate.
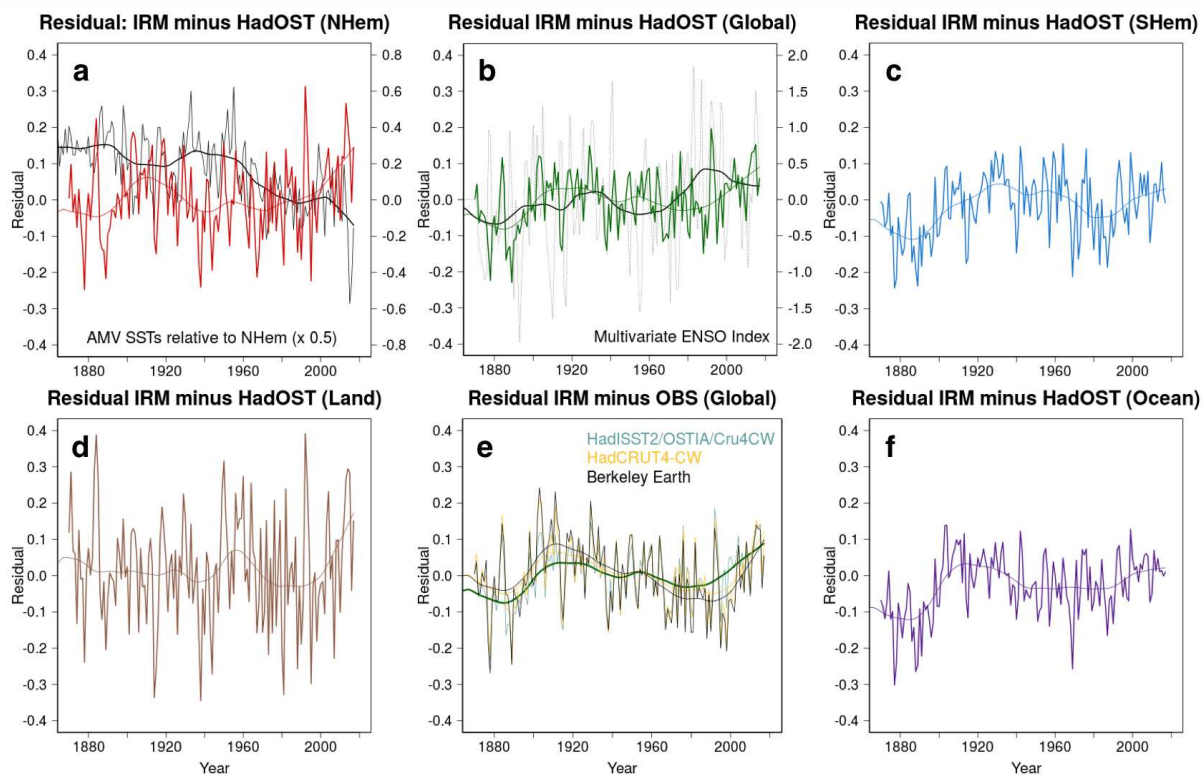
FIG. 7. Unforced residual observed variability. Impulse Response Model (IRM) minus HadOST for NHem (a), Global (b), SHem (c), Land (d), and Ocean (f). HadOST Global as in (b) is compared to CruCW4 and BE Global in (e). A 30 year lowess smooth is added in each plot. The revised AMV index is shown in (a). The Multivariate ENSO Index is added in (b). Note that the rhs y-axis labels for AMV (a) and MEI (b) are different.

68

Correlation Coefficient between (NHem) **Response Model, AMV and HadOST (1850-2016)**
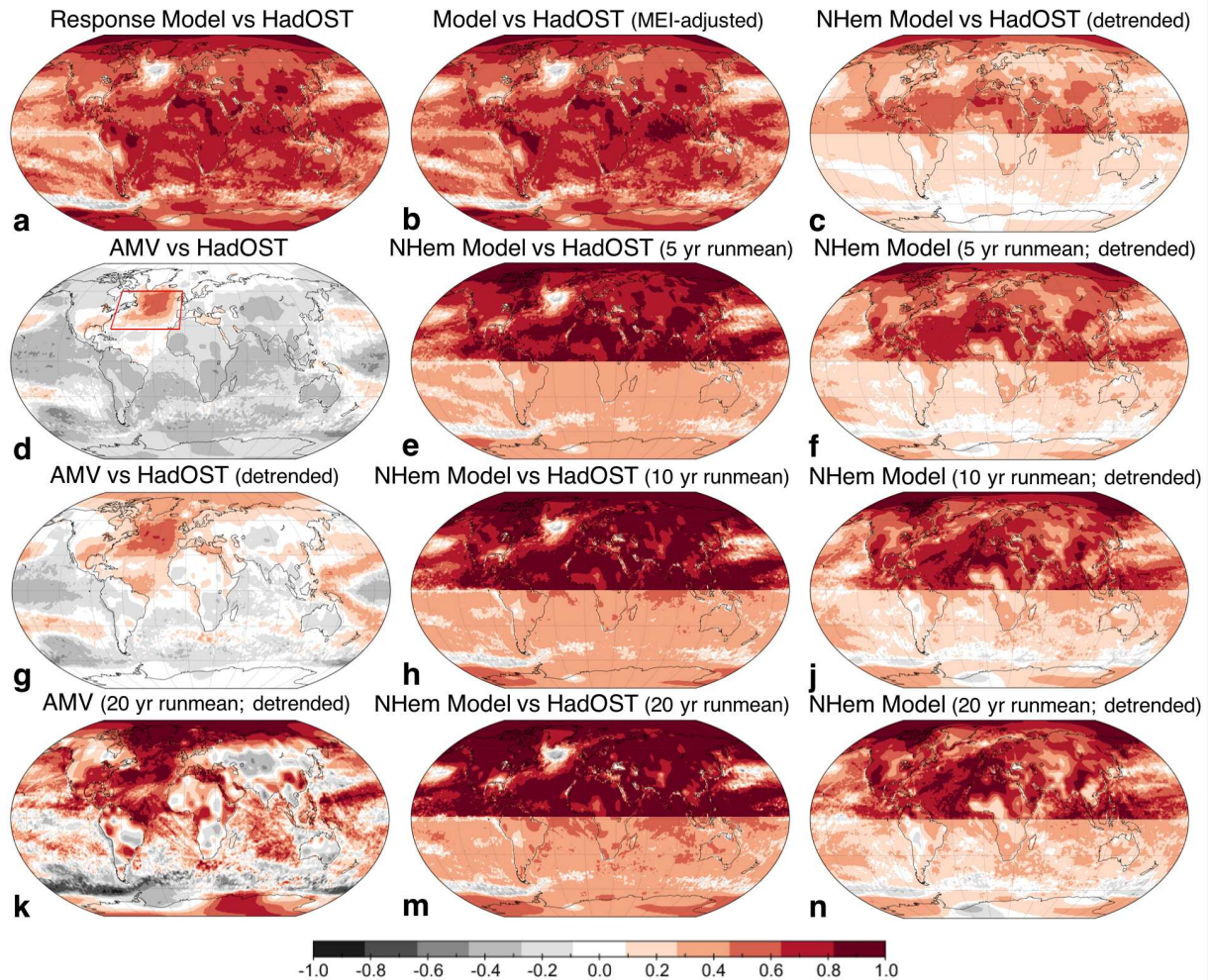
FIG. 8. Spatial map of correlation coefficients (R) over time between 1850-2016. Positive correlations in red and negative correlations in black. Annual means are used. (a) Time series of the global response model vs HadOST composite. (b) As (a) but with MEI noise added to the global response model time series. (c) Timeseries of the NHem response model vs HadOST. (d) The improved AMV index (van Oldenborgh et al. 2009) vs HadOST. The AMV/NAVI region is highlighted with a red box. (e) As (c), but with 5 year running means applied to both NHem and HadOST. (f) Combination of (c) and (e) where both regressors are detrended and low-pass filtered with a 5 year running mean. (g) As (d), but with both AMV and HadOST being detrended. (h) As (e) but with 10 year running mean. (j) as (f) but with 10 year running mean. (k) As (d), but with both AMV and HadOST being detrended and low-pass filtered with a 20 year running mean. (m) As (e) but with 20 year running mean. (n) As (f) but with 20 year running mean. SHem area is shown in semi-transparent colours to highlight the NHem region of interest.

Comparison of decadal air surface temperature averages (1850-2017)
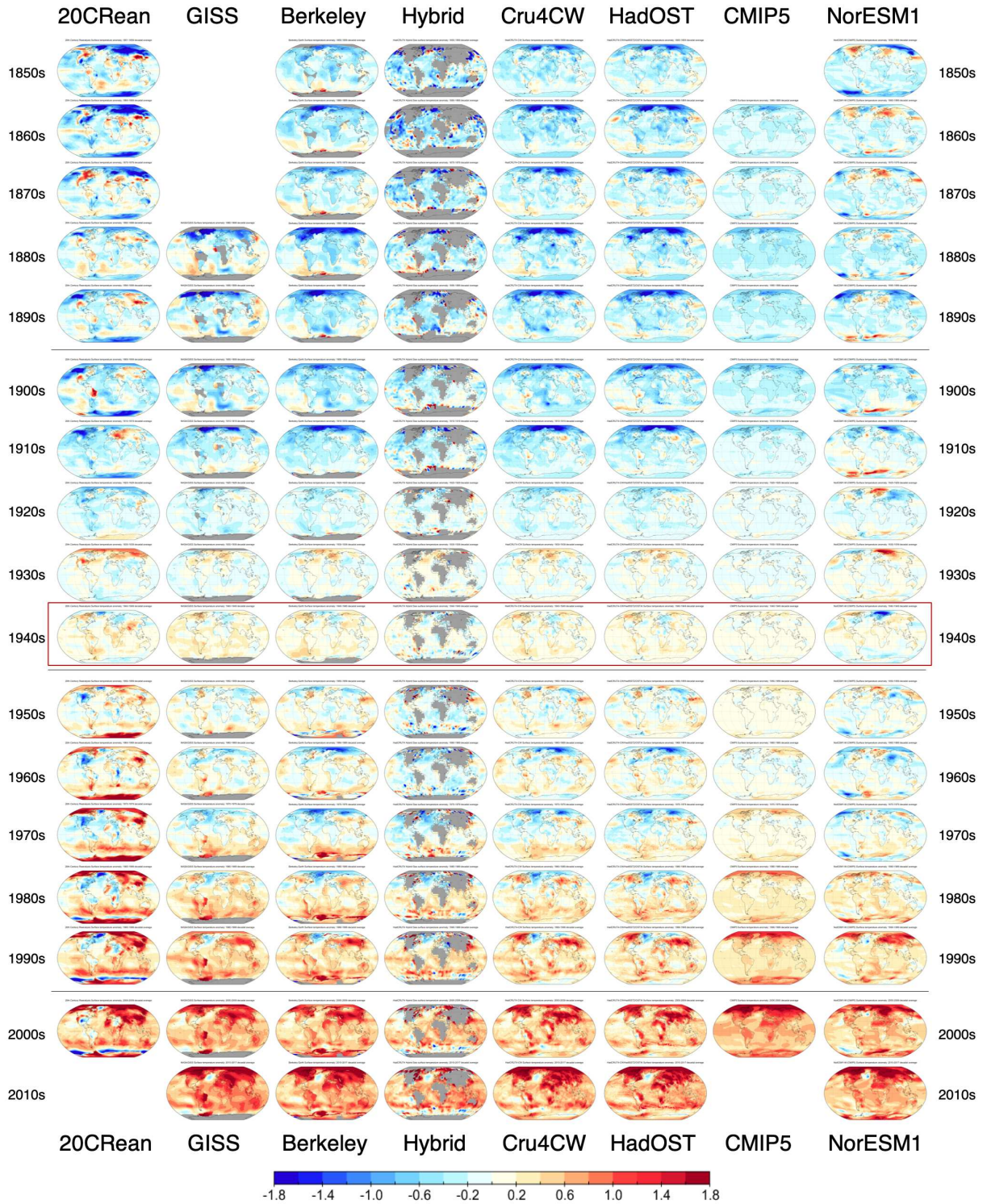
Fig. B1. Decadal GMST anomalies for the 20th century Reanalysis, all observational data used in this study including the new Hybrid SST dataset (Cowtan et al. 2017), CMIP5 subset and the NorESM1-M global circulation model. Decade from 1850-59 (top) to 2010-17 (bottom) are shown in each row. All anomalies are given relative to the 1901-2000 baseline period. The 1940-49 decade that is affected by the WWII warm bias is highlighted by the red box.